æ

18. RESOURCE ACQUISITION AND HOMEOSTASIS

23 March 2020

The most fundamental challenge of any organism is the acquisition of resources necessary for cell replication, without which the transmission of genes to the next generation is impossible. Cells must, of course, also avoid predation, infection, and other sources of mortality, but this requires resource investment as well. The goal here is to consider some of the evolved strategies that single-celled organisms exploit to harvest nutrients, often with extremely low environmental concentrations.

Nutrient acquisition takes many forms, from the direct uptake of small molecules from the environment to the fixation of carbon by photosynthesis to the engulfment of smaller cells by phagocytosis to the scavenging of host nutrients by intracellular parasites. Rather than provide an encyclopedic coverage of the topic, only the first two of these strategies will be considered in detail.

Although the molecular details can be quite complicated, relatively simple models have been developed to describe in mechanistic terms the basic response curves for uptake rates to ambient nutrient concentrations. These models highlight the key cellular features that need to be quantified to understand the basis for interspecies differences in nutrient-uptake parameters, and unfortunately point to substantial gaps in our knowledge. Photosynthesis is of particular interest as it fuels the biological world, and yet has unexplained inefficiencies.

Finally, because all cellular machinery has optimal operating conditions, homeostatic mechanisms exist to keep internal physiological conditions (e.g., ion balance) relatively constant in the face of a variable external world. A brief overview will be given for two such mechanisms – osmoregulation and the maintenance of an internal physiological clock. In both cases, crude estimates can be made of the energetic costs of homeostasis.

Elemental Composition of Cells

To provide baseline insight into the requirements for cellular, we start with the elemental composition of cellular biomass. Numerous surveys have been done on the elemental makeup of cells, especially in phytoplankton species, although quantitative analysis of the rarest trace elements are scant. Ignoring water (and other hydrogen and oxygen), carbon is always the predominant element in terms of molar composition, followed by nitrogen (Table 18.1). The bulk of the remaining biomass

is associated with the two other elements incorporated into one or more building blocks of cells (e.g., nucleic acids, amino acids, and lipids) – phosphorus and sulfur, along with five other major ions (e.g., sodium, calcium, magnesium, potassium, and chloride). All of these elements generally have intracellular concentrations > 1 mM/liter. Essential trace metals (e.g., iron, manganese, cobalt) that serve as cofactors of individual enzymes are present at one to two orders of magnitude lower concentrations. The classical view, first proposed by Redfield (1934), is that the ratio of C, N, and P atoms in cells is typically on the order of 106:16:1, and the average of the exemplars in Table 18.1, 100:13:1, is close to this expectation.

A comparison of cellular elemental concentrations with those in the environment reveals the effort that cells must go to sequester nutrients. There can be considerable variation in the biogeochemistry of different environments, but reliable average estimates exist for the inorganic content of ocean water (from which many of the species in Table 18.1 derive). The degree of cellular enrichment (in terms of molar concentration) is $\simeq 5000\times$ for carbon, and $50,000$ to $60,000\times$ for nitrogen (as nitrate, nitrite, and ammonia) and phosphorus (as inorganic phosphate). All of the remaining major ions range from being nearly isotonic with sea water to being enriched by no more than $25\times$. On the other hand, several essential trace metals (iron, manganese, and cobalt) are enriched by factors $> 10^6$.

To appreciate the challenges imposed by nutrient acquisition, consider as an example phosphorus, which has an average cellular enrichment of $\sim 60,000\times$. Living in an average marine environment, in order to produce an offspring, a bacterial cell with volume $1\,\mu\text{m}^3$ would need to accomplish the equivalent of fully clearing a surrounding volume of $\sim 60,000\,\mu\text{m}^3$ of P, and for the trace metals noted above, the equivalent of $\sim 10^6$ cell volumes would need to be scrubbed clean. For a moderate sized eukaryote, $100\,\mu\text{m}^3$ in volume, the necessary volumes of environmental clearance are $100\times$ higher.

When viewed in the context of cell-division times, the impressive rate at which cells harvest nutrients becomes clear. Again, consider a cell with volume 1 μm^3 (equivalent to 10^{-15} liters) at birth. With an average internal concentration of 115 mM/liter for phosphorus (Table 18.1), such a cell would contain $\sim 7 \times 10^7$ P atoms. Cells of this size have a minimum doubling time of ~ 0.4 days at 20°C (Lynch et al. 2020), implying an incorporation rate of ~ 2000 P atoms/sec at maximum growth rate. Similar calculations for cells of volume 10, 100, and 1000 μm^3, growing at maximum rates, indicate incorporation rates of $\sim 1 \times 10^4$, 9×10^4, and 6×10^5 P atoms/sec. Given the average 100:13:1 ratio for C:N:P noted above, these incorporation requirements would be 100 and $13\times$ higher for C and N atoms, respectively. Thus, depending on their size and temperature, when growing at maximum rates, cells incorporate on the order of 10^6 to 10^{10} atoms per minute.

As can be seen in Table 18.1, there is substantial variation among species in elemental composition, and some of this may relate to cell size. Menden-Deuer and Lessard (2000) summarized the scaling of carbon content with cell volume in a wide variety of unicellular marine eukaryotes. Aside from chrysophytes, which have inexplicably low carbon estimates, the average exponent on the power-law relationship across groups is 0.91 (SE=0.03), so there is a decline in carbon content per cell volume in larger cells. For cells of volume 1, 10, 100, and 1000 μm^3, mean carbon contents are 0.30, 0.23, 0.18, and 0.14 pg/μm^3. From Chapter 7, the average dry

weight of a cell is 0.5 pg/μm^3, so these results also suggest fractional contributions of carbon to dry weight of between 60 and 28%. A rough rule of thumb from these and other studies (Ho and Payne 1979; Roels 1980; Finlay and Uhlig 1981; Williams et al. 1987; von Stockar and Marison 1989; de Queiroz et al. 1993) is that carbon contributes about 45% to average dried biomass in both prokaryotes and eukaryotes.

Table 18.1. Contents of the major elemental constituents (other than hydrogen and oxygen) in a variety of unicellular species. Concentrations in the top half of the table are in units of mM, whereas as those in the bottom half are listed as μM. Species are in order of increasing cell volume (μm^3). The means for Ca and Sr exclude the haptophytes *E. huxleyi* and *Gephyrocapsa oceanica,* which have hard outer shells consisting of these elements. *Prochlorococcus* and *Synechococcus* are cyanobacteria; *Vibrio* and *Escherichia* are heterotrophic bacteria; *Pycnococcus, Nannochloris, Pyramimonas,* and *Dunaliella* are green algae; *Saccharomyces* is budding yeast; *Nitzschia, Amphidinium,* and *Thalassiosira* are diatoms; and *Prorocentrum* and *Thoracosphaera* are dinoflagellates. Seawater concentrations are taken from Nozaki (1997). References: cyanobacteria (Heldal et al. 2003); heterotrophic bacteria (Fagerbakke et al. 1996, 1999); yeast (Lange and Heijnen 2001); and all others (Ho et al. 2003).

Species	Size	C	N	P	S	K	Na	Mg	Ca	Cl
Prochlorococcus sp.	0.16	15323	1682	87	82	49	410	371	25	173
Synechococcus sp.	1.00	14906	1755	122	72	78	248	104	49	120
Vibrio natriegen	3.50	8333	1837	157	116	320	400	73	8	1320
Escherichia coli	3.80	7675	1880	263	74	62	210	61	10	104
Pycnococcus provasoli	10	14000	1900	72	77	89		19	4	
Nannochloris atomus	14	14000	2000	81	29	78		19	2	
Saccharomyces cerevisiae	67	15809	2218	131	27	39	7	26	0	
Nitzschia brevirostris	119	11000	1700	250	290	610		150	67	
Emiliania huxleyi	142	10000	1200	130	100	110		18	19000	
Gephyrocapsa oceanica	142	8900	1000	140	140	130		18	18000	
Dunaliella tertiolecta	227	11000	1900	49	14	18		18	1	
Amphidinium carterae	514	1200	160	9	12	1		5	3	
Pyramimonas parkeae	587	6800	570	32	47	27			55	
Prorocentrum mimimum	833	22000	1800	16	350	210		160	61	
Thoracosphaera heimii	1353	5100	400	63	82	63		30	2800	
Thalassiosira eccentrica	6627	18000	1900	240	470	790		520	160	
Means		11503	1494	115	124	167	255	106	232	429
Seawater		2.25	0.03	0.002	28	10.2	469	52.7	10.3	546
Cellular enrichment		5,100	50,000	57557	4.4	16.4	0.5	2.0	22.6	0.8

	Sr	Fe	Mn	Zn	Cu	Co
Pycnococcus provasoli	8	910	150	66	38	7
Nannochloris atomus	4	1100	93	140	19	7
Saccharomyces cerevisiae		354	31	642	46	
Nitzschia brevirostris	330	790	590	69	46	14
Emiliania huxleyi	44000	460	940	50	9	39
Gephyrocapsa oceanica	39000	560	990	57	16	50
Dunaliella tertiolecta	4	560	93	74	33	1
Amphidinium carterae	11	120	47	12	5	3

Pyramimonas parkeae	390	500	250	48	20	8
Prorocentrum mimimum	470	1100	980	140	440	73
Thoracosphaera heimii	5000	110	79	7	4	6
Thalassiosira eccentrica	950	1600	500	240	68	59
Means	796	680	395	129	62	24
Seawater	89	0.00054	0.00036	0.0054	0.0024	0.000020
Cellular enrichment	8.9	1,260,000	1,086,000	24,000	26,000	1,182,000

Adaptive fine-tuning of elemental composition? The basic building blocks of life, nucleotides and amino acids, vary in elemental content (e.g., C, N, P, and S), and this has led a number of authors to suggest that this provides a basis for adaptively tuning the elemental content of nucleic acids and proteins to prevailing environmental conditions through shifts in the use of alternative nucleotides and/or amino acids. Under this view, organisms living in environments depleted for one of these elements are expected to evolve towards under-representation of the same element in their building-block repertoires. In addition, pathways involved in the metabolism of a scarce element are expected to most strongly avoid the incorporation of the same element in the enzymes used in such reactions (Baudouin-Cornu et al. 2001; Alves and Savageau 2005; Acquisti et al. 2009).

For example, Baudouin-Cornu et al. (2001) found that enzymes involved in the assimilation of sulfur and carbon in *E. coli* and *S. cerevisiae* use amino acids that are, respectively, depleted with sulfur and carbon (e.g., methionine and cysteine in the case of sulfur). Similar claims have been made based on the absence of methionine and cysteine residues in cyanobacterial proteins expressed during times of sulfur depletion (Mazel and Marliére 1989), and based on nitrogen utilization in proteins in used for anabolism vs. catabolism (Acquisti et al. 2009). On the other hand, Baudouin-Cornu et al. (2001) found no such depletion for sulfur metabolizing enzymes in mammals, arguing that this is because mammals are less deprived of sulfur.

As the assumption underlying these arguments is that natural selection is powerful enough to discriminate among alternative building blocks differing in just one or two atoms of a particular type, it is worth examining whether the population-genetic conditions necessary for such selection are likely to be met. The matter can be evaluated by applying the general strategy outlined in Chapter 17, but in this case measuring costs in units of elemental composition rather than ATP equivalents.

Consider the use of carbon and nitrogen in nucleotides and amino acids. Over a range of growth conditions, the dry weight of *E. coli* cells consists of 45 to 47% carbon and 10 to 13% nitrogen (Folsom and Carlson 2015). The dry weight of an average cell in this species is ~ 0.00038 ng, which given the molecular weights of C and N, implies $\sim 9 \times 10^9$ C and $\sim 2 \times 10^9$ N atoms per cell. An A:T nucleotide pair contains 10 C and 7 N atoms, whereas a G:C pair contains 9 and 8, respectively. Thus, the exchange of an A:T for a G:C pair adds/subtracts just a single atom of each of these elements, changing the fractional elemental usages of C and N per cell by $\sim 10^{-10}$ and 0.5×10^{-9}, respectively. Given that no known species has an effective population size $> 10^{10}$, with N_e in *E. coli* being of order 10^9, such a shift

is expected to be barely detectable by natural selection. However, as most genes are represented by multiple copies of mRNA per cell, these numbers need to be multiplied accordingly. Nonetheless, because the average number of mRNA copies per cell per gene is < 10 in *E. coli* (Chapter 3), and unlike DNA, mRNAs are single-stranded, this still leaves the elemental cost very close to if not below the drift barrier.

In contrast, the maximum difference in C content among the 20 amino acids is 9 for tryptophan vs. glycine, and for N is 3 (arginine vs. several other residues). The maximum fractional impact of a single amino-acid substitution is then $\sim 10^{-9}$ for both C and N for a gene with just a single protein copy per cell for *E. coli.* However, for *E. coli,* the mean number of proteins per cell per expressed gene is $\simeq 2000$ with a very large standard deviation ($\simeq 5000$) (Lynch and Marinov 2015). This suggests that, at least in bacteria, the elemental costs of some amino-acid substitutions are in the realm of being detectable by natural selection, as the maximum fractional impact will often be in the range of 10^{-6} to 10^{-5}.

It is less clear that the conditions necessary for effective selection on elemental composition will commonly be met in eukaryotes. Because the average number of proteins per gene per cell increases less than linearly with cell volume (with the $\sim 2/3$ power, from Lynch and Marinov 2015), the cost/benefit of an amino-acid substitution might be expected to decline with cell volume. Thus, because N_e declines by two to five orders of magnitude from bacteria to eukaryotes, and cell volume increases by one to three orders of magnitude, it is questionable as to whether cellular elemental composition can be driven by natural selection in eukaryotes, especially in multicellular species with large cells. A simple alternative explanation for the mammalian results noted above is that the selective advantage of elemental change at the amino-acid level is too small to be visible to natural selection.

Nutrient Uptake Kinetics

Nutrient uptake rates are concentration-dependent. At low substrate concentrations, consumers are limited by resource encounter rates, whereas at high concentrations, uptake mechanisms become saturated. One of the simplest models for nutrient-uptake kinetics, which captures both of these effects, has the Michaelis-Menten form (derived for more general enzyme kinetics in Chapter 19, and identical in structure to the Monod growth equation in Chapter 9),

$$V = \frac{V_{\max} S}{k_S + S}, \tag{18.1}$$

where V is the rate of uptake of the nutrient (substrate) with concentration S, and k_S is the concentration at which V is 50% of it maximum value, $V_{\max}$. Written in this way, the rate of nutrient uptake describes a hyperbolic relationship between V and S, which closely approximates empirical results from hundreds of studies. The ratio $V_{\max}/k_S$, which is equal to the uptake rate per unit nutrient at low S, is commonly referred to as the uptake affinity. The model parameters $V_{\max}$ and k_S are simply summary descriptors of potentially complex cellular mechanisms, leaving

unexplained the actual determinants of such patterns. A more mechanistic model directly accounts for random encounter rates of the substrate by molecular diffusion and active transport across the cell membrane, while retaining the hyperbolic form of Equation 18.1 (Foundations 18.1).

Substantial attention has been given to nutrient-uptake parameters in phytoplankton species, particularly for nitrogen and phosphorus, which commonly limit growth in freshwater and marine ecosystems. The key parameters appear to be cell-volume dependent. Summarizing over a wide phylogenetic range of species, Edwards et al. (2012) found power-law exponents of 0.82 and 0.94 for $V_{\max}$ for N and P uptake, respectively, when scaled against cell volume, and exponents of 0.33 and 0.53 for k_S for these same elements. Uptake affinities ($V_{\max}/k_S$) for both elements also increase with cell size, the allometric scaling powers being on the order of 0.75 to 0.85. Similar results were obtained by Lomas et al. (2014) and Marañón (2015). Note, however, that although uptake affinities have positive allometric coefficients, implying that larger cells (on average) have higher rates of nutrient uptake on a per-cell basis, because the coefficients are < 1.0, on a per-biomass basis uptake rates actually decline with increasing cell volume.

What are the underlying determinants of these scaling features? In Foundations 18.1, it is shown that $V_{\max}$ is equivalent to the product of the number of transporters on the cell surface (per cell) and the rate of handling of substrate molecules by an engaged transporter. As the surface area of a cell is proportional to the square of the linear dimension, whereas cell volume is proportional to the cube of the latter, if the density of transporters per unit surface area remains constant, one would expect $V_{\max}$ to scale with the 2/3 power of cell volume (with variation around this expectation owing to shape differences). Some suggestion that such scaling occurs derives from observations on uptake rates for several amino acids in a polyploid series of yeast cells (from haploidy to tetraploidy) that increase in cell volume but are otherwise isogenic (Hennaut et al. 1970). However, the fact that the exponent (0.82 to 0.94) for interspecific comparisons is substantially higher than 0.67 suggests an increase in transporter density and/or a decrease in handling time with cell volume.

The half-saturation constant k_S also increases with transporter numbers and rate of handling (Foundations 18.1), albeit in a somewhat different way, so a positive scaling with cell volume is again expected. Why the allometric scaling of k_S is reduced substantially relative to that for $V_{\max}$ is unclear, but this could happen if the capture rates of transporters declined with increasing cell volume. In principle, the theory in Foundations 18.1 could be brought in closer alignment with empirical observations by directly evaluating the relationship between transporter number and the geometric features of cells, but the necessary empirical work remains to be done.

Although these kinds of scaling relationships may explain a number of aspects of variation in nutrient-uptake capacity based on purely structural arguments, there has been considerable speculation on the adaptive designs of various sized cells for particular environments (e.g., Chakraborty 2017), with Litchman et al. (2007) arguing that the uptake kinetics of various phytoplankton groups were essentially permanently molded by the physical/chemical environments in which the groups emerged phylogenetically, generally hundreds of millions of years ago. However, this frozen-phenotype view belies the rapidity with which metabolic processes can evolve in microbes (Helling et al. 1987; Maharjan et al. 2007; Blount et al. 2012; Samani

and Bell 2016).

Channels and transporters. Lipid membranes are essentially impermeable to the kinds of ions and organic molecules that cells harvest and export for nutritional and homeostatic reasons. However, for nearly every type of essential molecule, there exist specialized trans-membrane proteins dedicated to selective transmission across the lipid bilayer. Relative to cytoplasmic proteins, such molecules can be viewed as being inside-out, in the sense that the exterior of the transmembrane domain is hydrophobic (to enable embedding into the lipid environment), whereas the channel interior is hydrophilic.

Cellular investments in membrane proteins are enormous, with ~ 20 to 35% of genes in prokaryotes and eukaryotes encoding for them (Wallin and von Heijne 1998; Stevens and Arkin 2000). Because many types of channels are found across the Tree of Life (Greganova et al. 2013), they must have originated very early (pre-LUCA), e.g., potassium channels (Loukin et al. 2005), and aquaporins (Abascal et al. 2014). On the other hand, many have been lost from specific lineages and dramatically expanded in others. For example, potassium channels are absent from fission yeast, present as just one copy in budding yeast, but have expanded to ~ 300 copies in *Paramecium.* Losses of transporters are particularly common in parasite lineages, which can, for example, obtain nitrogen-containing amino acids and nucleotides from their host cells, eliminating the need for ammonia used in biosynthesis.

Although hydrophobic transmembrane domains are a key requirement for reliable membrane insertion, the barrier to such a condition may not actually be too great, as numerous studies have found that small random peptides often spontaneously develop into α-helices that adhere to the surfaces of lipid bilayers and under some conditions even insert as bundles of several helices (Lear et al. 1988; Pohorille et al. 2005; Mulkidjanian et al. 2009). Part of the reason for the enhanced stability of α-helices when aligned along membranes is the partial sheltering of their hydrogen bonds from open water. Thus, for biophysical reasons alone, proto-channels may have been quite feasible in the earliest stages of cellular evolution.

Membrane pores can be roughly partitioned into two categories. Channels are selective, sometimes gated, sieves that allow the transmission of some molecules, while excluding others. As they do not bind molecules directly, ion transfer through channels can approach the rate of diffusion. In contrast, transporters bind cargo directly, which reduces rates of molecular transmission down to levels in the range of 50 to 250 molecules per second, although most of the data are restricted to *E. coli* (Waygood and Steeves 1980; Naftalin et al. 2007) and yeast (Kruckeberg et al. 1999; Ye et al. 2001). Whereas channels operate in a passive manner and can only transport solutes down a concentration gradient, traffic through transporters requires energy to induce the structural changes necessary for opening and closing the pores on opposite sides of the membrane.

There are many ways by which transporters exploit energy inputs for the membrane passage of substrates. Many transporters couple the power from downhill diffusion of one molecule to the uphill work required for the import of a second molecule. Others cotransport protons or sodium ions (by the proton/sodium motive force) to drive cargo import. ABC (ATP binding cassette) transporters, found throughout bacteria and eukaryotes, utilize the energy from ATP hydrolysis to pump

substrates against a concentration gradient. The exact number of ATP hydrolyses per substrate molecule is not firmly established, but is thought to be near two, the same as the number of ATP-binding domains per transporter (Higgins 1992). Bacteria can also produce solute-binding proteins (SBPs) that sequester substrate molecules and then pass them on to cognate transporters (Driessen et al. 2000). In Gram-negative bacteria (with two membranes), the SBPs float freely in the periplasm, whereas in Gram-positives they are anchored to the cell surface.

Given the energy requirement for substrate movement, as well as the expense of producing the membrane proteins themselves, it is desirable to know the costs involved in import, as this must influence the success/failure of specific organisms in different environments. Although the requisite information for making such calculations appears to be lacking, it is clear what needs to be done. Knowing the number of atoms of a particular element comprising a newborn cell and the cell-division time, the total rate of cellular import can be computed (as done in the previous section), and if one is willing to assume an energetic cost per imported molecule (e.g., two ATP hydrolyses per molecule), the total cost of the import process can be computed. If one knows the rate of transport per channel, one can also estimate the number of channels necessary for such transport, and given a knowledge of the proteins involved, the cost of synthesizing the transporters themselves can be estimated.

Using this approach for *E. coli,* Phillips and Milo (2009) estimated that at saturating glucose concentrations (with an assumed transport rate of 100 glucose molecules/transporter/sec), $\sim 4\%$ of the membrane areas of these species must be allocated to glucose transporters. Assuming a 40 minute lifespan, and $\sim 2 \times 10^9$ glucose molecules to build a new cell, this implies: 1) a total cellular uptake rate of $\sim 833,000$ glucose molecules/sec, which at a transport rate of 100 molecules/sec, implies the presence of $\sim 8,000$ glucose transporters per cell; 2) a cost of uptake per cell division of $\sim 4 \times 10^9$ ATP hydrolyses (assuming a cost of two ATPs per imported glucose molecule), which is $\sim 13\%$ of the total cost of building and *E. coli* cell; and 3) a cost of import per transporter of $500,000$ ATP hydrolyses per cell division. This further suggests that the cost of import greatly exceeds the cost of building the transporters, as even a 1000 residue protein costs $< 10,000$ ATP hydrolyses (Chapter 17). All of these calculations are extremely rough, and further progress will require detailed direct observations on numbers of transporters per cell, transport rates, and energetic costs of transport per cargo molecule.

Physiological acclimation. Care should be taken in the interpretation of estimates of nutrient-uptake parameters, as these are often derived from cells in various states of physiological acclimation, and it is known that uptake affinities can be developmentally variable. When cells are acclimated to different nutrient conditions, and then assayed over a full range of nutrient concentrations, k_S is typically lower for cells previously exposed to nutrient-depleted medium (Collos et al. 2005), i.e., substrate affinity increases as the acclimation concentration decreases. In many species, such physiological responses are associated with the deployment of dual high- and low-affinity transporters, with the former being up-regulated in low nutrient conditions (Eide 2012).

Empirical observations in *S. cerevisiae* led Levy et al. (2011) to suggest that

dual-transporter systems enable cells to more effectively respond to shifts to nutrient-depletion conditions. The idea here is that low-affinity transporters activate a starvation response more readily than do high-affinity transporters, and in doing so enhance the expression of high-affinity transporter genes, thereby enabling the cell to endure a longer period of nutrient scarcity. What remains unclear, however, is why the same dynamical response could not be achieved with a single high-affinity transporter system by simply up-regulating the transporter concentration with decreasing nutrient abundance.

An alternative explanation that may solve this puzzle invokes a tradeoff between the maximum rate of uptake and k_S in different isoforms (Gudelj et al. 2007), such that with limited membrane space available for transporters, the one with the highest affinity at the current substrate concentration is utilized. Such a tradeoff might arise as a consequence of most transporters operating in a bidirectional manner (Figure 18.1). At high nutrient concentrations, high-affinity transporters can be saturated on both sides of the cell membrane, causing nutrient efflux to compete with influx, whereas low affinity transporters experience asymmetry (Bosdriesz et al. 2018). The resultant model, which allows the transporter binding-site conformation to switch from one side of the membrane to the other, leads to a modification of the normal Michaelis-Menten uptake kinetics. In contrast to uptake always increasing with the external substrate concentratio, bidirectional flow results in a situation where for any particular transporter k_S, there is a substrate concentration at which the uptake rate is maximized. With the optimum concentration increasing with decreasing affinity (Figure 18.1), the model then predicts that at higher external nutrient concentrations, lower-affinity transporters have higher rates of influx simply because they experience less conflict with internal cell concentrations.

Because genomes typically only encode for a small number of transporters for particular substrates, often no more than two, some peculiar behavior can arise under this model. Due to the existence of an optimal k_S for peak influx at any external nutrient concentration, the model predicts that for two transporters with k_S flanking the peak, there will always be a nutrient concentration at which both have equivalent influx rates. Notably, Wykoff et al. (2007) suggest that dual-transporter systems can exhibit bistable states, wherein at particular nutrient concentrations, a polymorphic (but clonally uniform) population of cells can be maintained. Although these authors view this sort of scenario to be the result of natural selection favoring a strategy for anticipating different types of nutrient-level changes, such an outcome may be nothing more than a physical consequence of the nature of the system.

Advantages of mobility. As discussed in Chapter 16, many microbes swim, with average rates in bacteria being in the range of 10 to 100 μm/sec and those in eukaryotic microbes being more on the order of 100 to 1000 μm/sec (Figure 16.4). There are numerous contexts in which swimming might confer an advantage, including predator avoidance, mate acquisition, and habitat selection. In raptorial species, motility will also increase the encounter rate of prey (Foundations 18.2).

To what extent might swimming increase the rate of uptake of passively diffusing molecules? Recall that small ions have typical diffusion coefficients in the range of $D = 70$ to 200 μm^2/sec, with an average value of 130 μm^2/sec (Figure 7.8). If swimming is to substantially increase the rate of nutrient uptake, the product of

the velocity (v) and the average distance between particles ($\overline{\ell}$), which has units of μm^2/sec, should exceed the diffusion coefficient of the harvested particles. Purcell (1977) called the ratio $\overline{\ell}v/D$ the stirring number (see also Zehr et al. 2017).

Assuming a random distribution, the mean inter-particle distance can be approximated as $[3/(4\pi S)]^{1/3}$, which is equivalent to the radius of a sphere having a volume per particle equal to the inverse of the substrate concentration, $1/S$. A concentration of 1 mM, roughly the situation for inorganic carbon in seawater (Table 18.1), contains $\sim 600,000$ particles/μm^3, which implies an average distance between particles of $\overline{\ell} = 0.007$ μm. To match the average rate of ionic diffusion noted above, such that $\overline{\ell}v = D$, the swimming velocity would then need to be $\sim 18,600$ μm/sec. Similar calculations for a concentration of 1 μM (two to thirty times lower than average N and P concentrations in the ocean) lead to a critical speed of $\sim 1,860$ μm/sec, and for 1 nM (similar to the concentrations of a number of trace metals) the critical speed is ~ 186 μm/sec. Because cells swimming in low Reynolds-number environments drag along most of their boundary layer as they move (Berg and Purcell 1977), these are likely lower-bound estimates of critical swimming speeds. In addition, no consideration has been given to the energetic cost of swimming.

The overall implication here is that swimming by microbes generally does not greatly magnify the rate of intake of randomly distributed inorganic nutrients. Large organic compounds such as proteins have diffusion coefficients roughly 10× those of inorganic ions, which would reduce the critical swimming velocities ten-fold, so depending on the environmental concentrations there may be some significant increases in their encounter rate. More likely, motility plays a central role in active searches for resources by following gradients by chemoreception (Chapter 22).

Photosynthesis

Whereas the previous section focused on the acquisition of dissolved nutrients, the global ecosystem largely depends on the conversion of solar energy into chemical energy that can be more directly used in the biosynthesis of organic materials. Organisms capable of such transformations are called photoautotrophs, in contrast to heterotrophs, which require reduced carbon compounds produced by the former. In addition to photosynthesis, five other carbon-fixation mechanisms are known to be exploited by various groups of anaerobic prokaryotes (Thauer 2007; Berg et al. 2010; Fuchs 2011). However, $\sim$ 99% of total global primary production is generated by RuBisCO, the key carbon-fixation enzyme in photoautotrophs (Raven 2009). A large fraction of the organic compounds produced by photosynthesizers are eventually taken up by heterotrophs, either via uptake as single molecules or by bulk ingestion by phagocytosis or herbivory.

Although photosynthesis is known to occur in seven bacterial phyla, only in the cyanobacteria and photosynthetic eukaryotes does it release oxygen. The diverse groups of photosynthetic eukaryotes (e.g, land plants, green algae, red algae, diatoms, dinoflagellates, euglenoids, and haptophytes) all owe such abilities to an ancestral endosymbiotic event involving a cyanobacterium (Shih 2015; Fischer et al. 2016; Chapter 23). The origin of oxygenic photosynthesis was a key moment in the Earth's history, as it provided a means for exploiting a permanent and reliable

supply of light energy to extract electrons from a highly plentiful molecule, water, and using these to produce ATP and NADPH necessary for the downstream synthesis of organic matter. In contrast, anoxygenic phototrophic prokaryotes rely on much rarer reduced inorganic compounds such as ferrous iron, hydrogen, and sulfur. Because the atmosphere of the early Earth was anoxic but had a plentiful supply of CO_2, with concentrations $100\times$ higher than in today's atmosphere (Raven et al. 2017), it is likely that anoxygenic photosynthesis was the first established form of photoautrophy. Indeed, given its phylogenetic distribution across bacteria, it may have been present in the ancestral bacterium (Woese et al. 1985; Woese 1987), with many lineages subsequently experiencing loss and transition to heterotrophic life styles.

The later emergence and phylogenetic spread of oxygenic photosynthesis had a profound effect of the Earth's history, leading to a 10^5-fold rise of atmospheric O_2 concentration and a smaller, but still substantial, reduction of CO_2 (Figure 18.2). The first big oxygenation event, occurring ~ 2.5 billion years ago and presumably a result of the origin of photosynthetic cyanobacteria, dramatically raised the atmospheric O_2, albeit to a level that was $\simeq 5\%$ of today's atmosphere. This set the stage for the widespread evolution of oxygenic metabolism by aerobic heterotrophs (Lyons et al. 2014). This approximate atmospheric state was maintained until ~ 750 million years ago, at which point there was a further elevation of O_2 concentration to today's level, presumably a consequence of the origin of photosynthetic eukaryotes. Over this period, there was a gradual draw-down of atmospheric CO_2 to today's level (which is several-fold lower than that 1 million years ago).

The transformation of solar to chemical energy. As almost all photosynthesis is carried out by aerobes, the focus here will be on oxygenic photosynthesis. The details of this complex system are outlined in most biochemistry texts, and only a gross overview is provided here. The transition to oxygenic photosynthesis involved two major innovations: 1) the water-oxidizing photosystem II releases electrons, protons, and oxygen; and 2) photosystem I utilizes the electron/proton output from photosystem II to drive the production of the energy carrying compounds ATP and NADPH.

The two photosystems are thought to have originated by duplication and divergence events deep in the bacterial phylogeny, although the sequence similarity of their molecular constituents is so low as to raise considerable uncertainty on this interpretation. Although photosystems I and II are each sequestered in three non-cyanobacterial groups, the two systems coexist only in the cyanobacteria. Thus, a key question is whether photosynthetic cyanobacteria joined the two systems via a horizontal transfer, or whether the dual system is ancestral with other lineages experiencing losses. Because all lineages of anoxygenic photosynthetic bacteria appear to be derived within their phylogenetic groups, with no evidence for ancestral phototrophism within any group (even cyanobacteria) (Fischer et al. 2016; Shih et al. 2017), the most parsimonious explanation is that anoyxgenic photosynthesis is ancestral, with multiple horizontal-transfer events occurring deep in bacterial phylogeny, one of which led to the dual I/II system.

Both photosystems are comprised of complexes of twenty or so protein subunits and cofactors, which jointly carry out processes of light-harvesting, photoprotection,

and transfer of electrons and protons. Two of the major photosystem II proteins evolved by gene duplication prior to the diversification of the cyanobacteria and operate as heterodimers, whereas all bacterial photosystem I complexes operate as homodimers, except in cyanobacteria where they are heterodimeric (Cardona 2015; Cardona et al. 2015).

The overall process of photosynthesis is further subdivided into the light reactions (carried out by the photosystems just noted) and the downstream carbon-fixation dark reactions (somewhat of a misnomer, as they can occur in light and dark). The quantum efficiency of the light reaction of photosynthesis, defined to be the number of moles of photons (called Einsteins) absorbed per mole of oxygen produced, is sometimes viewed as a universal constant. However, there is continuing disagreement as to its actual value (Melis 2009; Hill and Govindjee 2014), and although most estimates are in the range of 8 to 10 photons per O_2, it remains possible that this number differs among phylogenetic lineages. Taking the average, ~ 9 photons are required to convert two H_2O and two $NADP^+$ into one O_2, two hydrogen ions, and two NADPH. The hydrogen ions generated by this reaction are used to drive the production of ATP from ADP using an ATP synthase embedded in the inner membranes of the chloroplast (in essentially the same way the analogous machine operates on the plasma membrane of bacteria and the inner mitochondrial membranes of eukaryotes).

The carbon-fixation (dark) reactions, also known as the Calvin-Benson cycle, consume three molecules of CO_2 to produce one triose phosphate molecule that can then be used in the synthesis of higher-order organic compounds. This is an energy intensive process, with each triose phosphate requiring the investment of six NADPHs and nine ATPs provided by the light reaction. This means that ~ 27 photons (4.5 per NADPH, from the preceding paragraph) are then required for the production of the six NADPHs per triose phosphate. If we assume that three protons are required for the production of each ATP, then 27 protons are required per triose phosphate. Noting that the latter requires ~ 122 photons (4.5 per hydrogen ion, from above), ~ 149 photons are required for the production of each triose phosphate.

Using chlorophylls a and b, along with a set of accessory pigments, all arranged in the large photosystem complexes contained within a reaction center, most photosynthesis relies on photons from the 400 to 700 nm wavelength range of the solar spectrum (essentially the visible spectrum). However, there is substantial energy available in the infrared range of sunlight that goes unharvested by most plants. A few photosynthesizers such as the cyanobacterium *Acaryochloris* have an accessory pigment that expands the range of availability up to 750 nm (Chen and Blankenship 2011), but it remains unclear why the vast majority of plants leave this resource untouched.

The world's most abundant enzyme. The centerpiece of photosynthesis is RuBisCO (ribulose-1,5-bisphosphate carboxylase/oxygenase), the enzyme that catalyzes the joining of ribulose-1,5-bisphosphate (RuBP) and CO_2 into a product that is subsequently split into two three-carbon molecules (3-phosphoglycerates). The latter are then deployed in downstream biosynthetic pathways as well as in the recycling of RuBP for another round of carbon fixation. RuBisCO is thought to be the most abundant protein on Earth, summing to $\sim 0.7 \times 10^{12}$ kg, 95% of which is

in terrestrial plants (Bar-On and Milo 2019).

Phylogenetically, the enzyme consists of two major variants: form I (eight large and eight small subunits) in all eukaryotic algae and cyanobacteria; and form II (no small subunits) in anaerobic photosynthetic proteobacteria and dinoflagellates, each of which has multiple structural variants (Morse et al. 1995; Erb and Zarzycki 2018). However, the evolutionary roots of RuBisCO are less clear. The presence of RuBisCO-like protein families with other functions in various bacterial and archaeal lineages suggests that CO_2-fixing RuBisCO may be derived from a protein with quite different features, possibly nucleotide assimilation (Ashida et al. 2005; Erb and Zarzycki 2018). Within eukaryotes, RubBisCO appears also to have experienced multiple horizontal gene-transfer events (Delwiche and Palmer 1996).

As already noted, photosynthesis is an energetically expensive process, and this point is further emphasized by the large size and enzymatic inefficiency of RuBisCO. With a turnover rate per catalytic site one to two orders of magnitude lower than typical enzymes, RuBisCO must be maintained at high intracellular concentrations. Moreover, relative to maximum-capacity measurements of RuBisCO in the laboratory, the global time-average performance of the enzyme in nature is just 1% for terrestrial and 15% for marine environments (Bar-On and Milo 2019).

RuBisCO is also remarkably error-prone. As implied by its designation as a carboxylase/oxygenase, the enzyme competitively binds both CO_2 and O_2, with the latter event resulting in the production of a toxic by-product that is eliminated by a process called photorespiration. The extraordinary error rate of RuBisCO, which can be as high as 20%, remains an enigma. The ability to discriminate between CO_2 and O_2, defined as $S = (V_{CO_2}/k_{CO_2})/(V_{O_2}/k_{O_2})$, is equivalent to the ratio of uptake affinities of the two substrates. Tortell (2000) suggested an inverse relationship between S and the estimated geological age of a phylogenetic group, with an increase from ~ 50 in ancient cyanobacterial lineages to 200 in more recent diatoms, although red algae are a clear outlier. As noted above, however, given the well-known ability of microbes to evolve metabolically on time scales of 1000s of generations, the likelihood of enzymatic features remaining frozen with suboptimal features for millenia seems very small. Moreover, the frozen-accident hypothesis is inconsistent with broad phylogenetic analyses suggesting substantial adaptive amino-acid substitutions in RuBisCO, including on the dimeric interfaces near the active sites of the enzyme (Kapralov and Filatov 2007; Young et al. 2012).

A common, alternative narrative is that the low efficiency and error-prone nature of RuBisCO is an inevitable consequence of structural constraints, with the enzyme actually having near optimal performance conditional on the unavoidable compromises. One motivation for this argument is the negative correlation between the catalytic affinity for CO_2 and the specificity factor of the enzyme, with each feature varying by more than an order of magnitude across species (Tcherkez et al. 2006; Savir et al. 2010; Shih et al. 2016; Flamholz et al. 2019). Cyanobacteria are at one extreme in having high maximum rates of carboxylation but low specificities, whereas the red algae are at the opposite end of the spectrum, with chlorophytes having intermediate values of both. Although the statistical relationship is on solid grounds, the proposed mechanistic constraint has not yet been demonstrated empirically, and the overall pattern might be viewed as an example of a bivariate drift barrier, with certain combinations of traits endowing species with similar net

carbon-fixation capacities.

There is in addition a third determinant of the efficiency of CO_2 utilization by RuBisCO. The realized ratio of CO_2 to O_2 catalysis is equal to the product of the specificity factor and the ratio of concentrations of the two substrates at the active site of RuBisCO. Many species enhance the latter via a CO_2-concentrating mechanism (CCM) for increasing the internal availability of CO_2 (Beardall and Giordano 2002; Falkowski and Raven 2007). Such mechanisms are most famous in land plants harboring C_4 and CAM (crassulacean acid) metabolisms. In these cases, CO_2 is incorporated into malate in spatially or temporally separate contexts from RuBisCO, which subsequently receives its CO_2 payload after malate dissociation. Malate formation appears to have been evolutionarily modified into a CCM many dozens of times independently in land plants (Brown et al. 2011; Heyduk et al. 2019), as well as in various algal lineages (Raven et al. 2017). For example, cyanobacteria concentrate CO_2 locally into microcompartments housing the photosynthetic apparatus (carboxysomes).

As an efficient CCM will offset a reduced specificity factor, this provides another potential example of a bivariate drift barrier, and indeed there is a strong inverse relationship between the specificity factor and CCM factor across species (Badger et al. 1998). Still another example of evolutionary compensation is the observation that species with high specificity factors produce less RuBisCO (Hobson and Guest 1983). Although these observations suggest potential strategies for engineering RuBisCO molecules with greater catalytic efficiency and speed, and numerous attempts have been made to improve the enzyme, for the most part there has been limited success (Spreitzer and Salvucci 2002; Gomez-Fernandez et al. 2018).

Osmoregulation

Although cells often experience dramatically different environments on within- and between-generation time scales, they go to extremes to ensure that internal physiological operating conditions remain relatively constant. Because the structure and function of proteins depends on their surrounding chemistry, to operate in an efficient manner, cells must regulate the concentrations of their constituents, including hydrogen ions and all other dissolved substances. Among other things, this raises the necessity of osmoregulation. Hyperosmotic (saline) environments promote cell dehydration, excess molecular crowding, and reduced levels of molecular diffusion. In contrast, hypoosmotic environments induce cell swelling and potential membrane rupture.

Water can pass through cell membranes at potentially very rapid rates, owing to the presence of membrane-spanning pores called aquaporins, which selectively (and passively) admit water molecules while excluding other ions. Because aquaporins are present across the entire Tree of Life, with the apparent exception of some thermophilic bacteria (Abascal et al. 2014), they were likely present in LUCA. In eukaryotes, they have diversified into two major groups, one of which engages in glycerol transport for reasons discussed below. The overall implication, however, is that aside from regulating the number aquaporin channels, much of osmoregulation must involve the active transport and/or production of solutes.

For bacterial cells completely surrounded by a cell wall, the natural tendency for cell-volume expansion by water entry is countered by the resistance of the cell wall. However, the resultant equilibrium turgor pressure by no means eliminates problems with osmotic stress. Because there are no active pumps for water molecules in bacteria, osmoregulation requires continual environmental sensing and, where necessary, rapid fluxes of ions and/or the synthesis of compatible solutes (Bremer and Krämer 2019). Compatible solutes are small organic osmolytes such as glycerol, proline, glycine betaine, and sucrose that have no effects on the performance of active molecules (i.e., are compatible) and can be rapidly expelled if the external medium is too hypoosmotic (Figure 18.3).

The power of cell walls for reducing the costs of osmotic balance is illustrated by a class of phenotypic variants in numerous bacterial species called L-form cells (Errington et al. 2016; Errington 2017; Claessen and Errington 2019). These wall-less cells are induced by chronic exposure to antibiotics that interfere with peptidoglycan production (e.g., phosphomycin and D-cycloserine). However, the maintenance of cultures of L forms requires an osmoprotective medium (usually achieved by the addition of sucrose, which is not metabolized). Given that many eukaryotic lineages have abandoned cell walls, long-term evolution experiments to gradually wean L-forms from dependence on a hyperosmotic environment would help illuminate the mutational emergence of secondary accommodations to such a radical change in cellular structure. Given the energetic costs of cell walls (Chapters 16 and 17), the development of stable cultures of such cells may also have utility in biotechnological applications.

Oren (1999) calculated the costs of osmoregulation in bacteria using compatible solutes vs. ionic balance. The compatible-solute strategy requires the intracellular synthesis of organic osmolytes, whereas the ion-balance strategy requires the flux of appropriate ions across the plasma membrane. Mixtures of the two strategies occur, and such regulation is especially important in marine and other hypersaline environments. Depending on the costs of alternative strategies, different species may be favored in some environments and excluded from others.

The biosynthetic costs per compatible-solute molecule (in units of ATP hydrolyses) range from 27 to 95, increasing with increasing molecular weight of the compound (Figure 18.3). Based on the molarity of compatible solutes in cells of marine microbes, this led Oren (1999) to suggest that up to 85% of the cost of a cell per division may be associated with osmoprotection. Given these substantial costs, it remains unclear why variation among organisms exists for the compatible solutes deployed. Glycerol is the cheapest solute to produce, and also has the highest solubility. However, although relied upon by the marine alga *Dunaliella,* which has specialized membranes, and yeast, glycerol is a challenge because of its ability to permeate most membranes. Many nonhalophilic bacteria utilize sucrose or trehalose.

Equally unclear is why most species rely on compatible solutes at all. Although the data are scant, most molecular work suggests that specialized transporters require one to two ATP hydrolyses for the forward movement of each transported molecule (Oren 1999; Patzlaff et al. 2003; Lycklama a Nijeholt 2018). Species that balance osmotic pressure with ion balance often do so by modulating the cellular concentration of KCl. Potassium and chloride are imported through specific trans-

porters, coupled with sodium export and proton input and utilizing ATP-dependent mechanisms. The cost of import appears to be on the order of 0.5 to 0.67 ATP hydrolyses per KCl imported, which is 40 to 190× lower than the cost of synthesizing a compatible-solute molecule. Note, however, that these calculations do not include the costs of the machinery necessary to carry out these processes, which might be considerably greater in total for Na^+/H^+ antiporters and K uniporters than for the biosynthetic machinery for compatible solutes.

In the absence of turgor pressure, wall-less cells (most eukaryotes) face additional problems with osmotic pressure. To retain high levels of intracellular solutes, there is a need for a mechanism for removal of water molecules that work themselves through the membrane. This problem is magnified greatly in cells engaging in phagocystosis and the inevitable consumption of the external medium. Among flagellated eukaryotes, even walled cells have a water problem, as the flagella are surrounded by lipid bilayers (but not by walls) providing an entry for water molecules. Many eukaryotes deal with this relentless import of water by use of a contractile vacuole, which grows in volume by accumulating excess cell water, and then periodically ejects its contents into the surrounding medium. How this is accomplished in a way that selectively retains key cytoplasmic constituents remains unclear, although a number of hypotheses have been suggested (Raven and Doblin 2014).

The amount of water expelled by eukaryotic cells is impressive. For example, Lynn (1982) found a positive scaling of the volume of the contractile vacuole and cell volume in ciliates, with the total rate of volumetric output (μm^3/day) scaling as $460V^{0.88}$, where V is the cell volume (in μm^3). For the range of ciliate cell sizes studied, $\sim 10^4$ to 10^6 μm^3, this relationship implies that between 152 and 87 cell volumes of water are ingested (and expelled) per day. Even higher rates have been found in other organisms. For the green alga *Chlamydomomas reinhardtii,* with a cell volume of $\sim 140\,\mu m^3$ and an average expulsion rate of 38,000 μm^3/day (Raven 1982; Buchmann and Becker 2009), the implied number of cell volumes ingested per day is 270. Another green alga *Mesostigma viride,* which harbors eight contractile vacuoles, ingests 1150× its volume per day (Buchmann and Becker 2009).

An understanding of these demands can be obtained from expressions for the flow rate of water across a membrane of known porosity separating two liquids with different osmolarities (Foundations 18.3). Such analyses also lead to the conclusion that a very substantial fraction of eukaryotic cell maintenance requirements must be devoted to osmoregulation. The overall implication here is that, owing to different osmotic demands and the evolved mechanisms for dealing with them, the growth performance of organisms in environments with different salinities may be substantially altered even in the face of equivalent levels of availability of critical resources.

Circadian Rhythms

Most multicellular organisms have internal molecular clocks, called circadian rhythms, that enable them to anticipate light-dark phases and make appropriate physiological changes. In effect, such time keepers enable organisms to predict the short-term future and make changes in gene expression appropriate to the demands of day/night

environmental conditions. Most multicellular organisms have generation lengths of weeks to years, so such diurnal cycles occur many times throughout the life of the individual. However, in unicellular species, minimum cell-division times can be much less than 24 hours. Individuals then commonly complete their entire lives in very different periods of the diurnal cycle, raising questions as to the utility of a molecular clock in such species. Nevertheless, they do exist.

The definition of a circadian system is somewhat subjective, but the central feature is some form of robust rhythmicity, with a near 24-hour periodicity that can be accurately entrained by an external factor (such as a light:dark cycle) but can also remain free-running for extended periods in a constant environment. A lack of the periodicity's sensitivity to absolute temperature (unlike most biochemical properties) is generally taken to be a hallmark of a true circadian rhythm. Evidence for such rhythms has been found in numerous unicellular phototrophs including green and red algae, dinoflagellates, and euglenoids (Roenneberg and Merrow 2001; Brunner and Merrow 2008; Noordally and Millar 2015). Eelderink-Chen et al. (2010) found that imposition of a temperature cycle can entrain a circadian rhythm in the yeast *S. cerevisiae,* although the cycle is damped within just two days of constant temperature. A day:night circadian rhythm is also loosely coupled to the mitotic cell cycle in the filamentous fungus *Neurospora,* albeit with cell division being far from synchronous (Hong et al. 2014). Although few of the details have been worked out, the time-keeping mechanism in all of these cases is thought to be governed by rhythmicity in clock-component gene transcription, as in land plants and metazoans. In multiple eukaryotes (humans, green algae, and filamentous fungi), rhythmicity appears to be governed by intracellular levels of magnesium, which operates as a cofactor with ATP and can therefore globally influence cellular features such as translation rates (Feeney et al. 2016).

Although the existence of entrainable clocks in nonphotosynthetic bacteria is circumstantial at best (Sartor et al. 2019), the cyanobacterium *Synechococcus* has well-characterized circadian clock, with a simple mechanism quite unlike that in eukaryotes. Indeed, the core oscillator can be made to operate *in vitro* in a solution containing just three proteins (KaiA, KaiB, and KaiC) and ATP (Nakajima et al. 2005; Phong et al. 2013). The oscillations are sustained by a cycle of post-translational modifications. The central hub, KaiC, is phosphorylated in the presence of KaiA, but once this occurs, KaiB forms a complex with KaiC that inhibits KaiA, thereby promoting dephosphorylation of KaiC, starting the cycle anew. This cycle further elicits a signal-transduced cascade (Chapter 22) of gene-expression events that favor growth-inhibition in the absence of light. Also of note is that KaiC is a homo-hexamer. Although the phosphorylation of individual molecules is a stochastic process, the hexamers dissociate and reassociate, leading to homogenization of their phosphorylation states and hence a more coherent signal (Kageyama et al. 2006).

The *Synechococcus* clock is different from that typically observed in eukaryotic systems, which are generally based on negative feedback resulting from activating genes whose products ultimately repress their own expression. The cycle seems to be set by metabolic oscillations determined by diurnal resource availability, and hence is only indirectly correlated with the light:dark cycle itself (Pattanayak et al. 2015). Moreover, as with the clocks of land plant and animals, the *Synechococcus*

circadian rhythm can track changes in the day:night cycle even in an *in vitro* setting, providing a built-in response to seasonal changes (Leypunskiy et al. 2017). Artificial arrests of growth instituted by exposure to short pulses of darkness reset the clock in inappropriate ways, decreasing cell division rates (Lambert et al. 2016), and this raises a second issue.

A key challenge for circadian clocks concerns the sensitivity to internal and external noise. The former derives from small numbers of molecules per cell and bursty transcription, and the latter from weather effects such as cloud coverage. Internal noise is expected to be more significant for species with smaller cells, which naturally harbor smaller numbers of proteins. Thus, it is of interest that *Prochlorococcus,* a marine cyanobacterium that is significantly smaller than *Synechococcus,* does not have a free-running circadian clock like the latter, but instead an hourglass-like clock, which responds directly to each daily change in light:dark and does not run freely in the absence of a daily signal. This shift is a consequence of the absence of the negative-feedback component KaiA in this species (Holtzendorff et al. 2008).

There is indirect evidence that this kind of shift in clock structure may be adaptive in small-celled species (rather than simply being a consequence of genomic streamlining). When the internal noise is sufficiently large, free-running clocks are perturbed enough by noise amplification in the negative-feedback loop to become more unreliable than hourglass clocks, which are naturally reset each day. On the other hand, the former appear to be less vulnerable to large-amplitude fluctuations in external signals (Chew et al. 2018; Pittayakanchit et al. 2018). The effects here are not large, however, and it remains to be shown whether the stochasticity of the clocks in these alternative systems have adaptive consequences.

The total cost of running and maintaining a molecular clock remains to be determined, but in the example given above, progress can be made, as it appears that the vast majority of the cost is associated with the biosynthesis of the proteins involved. The Kai system is driven by ATP hydrolysis, but the 24-hour cycle is driven by the hydrolysis of just 60 ATP molecules per hexamer (Terauchi et al. 2007). Because each monomer of the KaiC hexamer consists of 518 amino acids, with a biosynthetic cost of a few ATP hydrolyses per amino acid, provided the cell-division time is a day or less, it is clear that the biosynthesis of the Kai components constitutes almost all of the cost.

Chew et al. (2018) estimate the numbers of molecules/cell to be $\sim 4,000$ for KaiA (284 amino acids), $11,000$ for KaiB (102 amino acids), and $8,000$ for KaiC. Assuming a total cost of ~ 30 ATPs per amino acid, implies a total biosynthetic cost $\simeq 2 \times 10^8$, as compared to the $\sim 5 \times 10^5$ for running the clock. Using the expression from Lynch and Marinov (2015), the cost of building a *Synechococcus* cell (with volume $\sim 0.5\ \mu\text{m}^3$) is $\sim 14 \times 10^9$ ATP hydrolyses, so on the order of 1.5% of the energy budget is consumed by building and running the clock.

A similar computation can be made for the diminutive marine green alga *Ostreococcus,* which has a cell volume $\simeq 1.7\ \mu\text{m}^3$, and therefore requires $\sim 45 \times 10^9$ ATP hydrolyses to build a cell. The clock in this species runs by a simple transcriptional-loop mechanism, with one protein (CCA1) repressing the transcription of another (TOC1), and the latter activating transcription of the former (Bouget et al. 2014). The circadian cycle is driven by protein degradation, with the number of CCA1 protein copies cycling from 100 to 400 per day, and of TOC1 proteins cycling from

10 and 150 per cell (van Ooijen et al. 2011). Thus, the protein degradation rates are 0.75 and 0.93, respectively. Letting the proteins be $\sim$ 300 and 500 in length, and assuming one cell division per day, using Equation (4) from Lynch and Marinov (2015), which assumes amino acids are recycled, leads to estimates of total costs of protein production of 3.6×10^6 and 2.2×10^6 ATP hydrolyses for CCA1 and TOC1, respectively, which is on the order of just 0.01% of the cell's total energy budget. A number of costs are ignored here, but their inclusion would be unlikely to increase this estimate by more than an order of magnitude. For example, although the cost of transcription has been ignored, this is known to be on the order of 10% of the protein-level cost. The clock in this species seems to run via non-transcriptional rhythms of a light-sensitive protein (O'Neill et al. 2011), which could further increase the cost several fold.

The central point, however, seems to remain – the overall cost of running a clock in this species is kept very small because of the low number of proteins involved. Recall, however, that were there to be an advantage of losing a clock, a bioenergetic advantage of 1% would be quite easily promoted by natural selection.

Summary

- Most cells require $\sim$ 20 elements for growth, many of which have cellular concentrations that are 10^4 to $10^6\times$ that in the surrounding environment. These enrichment factors are equivalent to the number of cell-volumes of surrounding bulk medium that must be cleared to produce an offspring cell.

- Nutrient-uptake affinities increase with cell volume across species on a per-cell basis, but decline on a per-biomass basis with increasing cell size. Although the data are limited, $>$ 10% of cell energy budgets is allocated to nutrient uptake, and many species adjust to their surrounding nutrient levels by deploying membrane-bound transporters with different levels of substrate affinity.

- The process of oxygenic photosynthesis, which is responsible for the fixation of almost all of Earth's carbon, is an energetically expensive process. It is carried out by RuBisCo, probably the world's most abundant but also one of the least efficient enzymes.

- To keep their internal conditions at near-optimal states for physiological function, all cells have a variety of homeostatic mechanisms. Osmoregulation is a perpetual problem for cells, as internal concentrations are generally hyperosmotic with respect to the external environment. Cell walls counter the osmotic stress confronted by many species, but wall-less species (many eukaryotes) must continually pump water out, often with the daily export equivalent to 100 to 1000$\times$ the cell volume. The relative costs of structural (wall) vs. dynamical (pump) solutions remain to be worked out, but both consume a considerable fraction of cellular

resources.

- A number of unicellular species have independently evolved internal circadian clocks that provide a basis for predicting and preparing for diurnal environmental changes. Although only understood in a few species, the molecular mechanisms appear to consume no more than 1% of a cell's daily energy budget.

Foundations 18.1. The response of uptake rate to nutrient concentration. The uptake of a molecule is typically carried out by specific membrane-bound nutrient transporters. The total rate of uptake by a cell is then expected to scale positively with the number of transporters residing in the cell membrane and the nutrient concentration at the surface of the cell. The latter, however, is not the same as the concentration in the bulk medium. As nutrients at the cell surface are constantly being taken up, there is a natural concentration gradient away from the cell surface governed by the rate of nutrient diffusion. Thus, one way of achieving a mechanistic understanding of the cellular rate of nutrient uptake is to first consider the transporter-based uptake kinetics conditional on the nutrient concentration at the cell surface, and then to relate the latter to the external diffusion process (Armstrong 2008).

Letting f denote the fraction of transporters on the cell surface engaged with a substrate molecule, t_h be the handling time of a captured molecule (the time to transport the molecule to the cytoplasm), k_c be the capture rate of a substrate molecule by an unengaged transporter (scaled to the nutrient concentration), and S_0 be the nutrient concentration at the cell surface, the rate of change in transporter occupancy is

$$\frac{df}{dt} = k_c S_0(1-f) - f/t_h. \tag{18.1.1a}$$

At steady state, $df/dt = 0$, giving a mean fraction of occupied transporters

$$\widetilde{f} = \frac{S_0}{[1/(k_c t_h)] + S_0}, \tag{18.1.1b}$$

which asymptotically approaches 1.0 as $S_0 \to \infty$. With n_T transporters per cell surface, and each engaged transporter handling its cargo at rate $1/t_h$, the total rate of nutrient uptake is then

$$V = \frac{n_T \widetilde{f}}{t_h} = \frac{V_{\max} S_0}{k_T + S_0}, \tag{18.1.2}$$

with $V_{\max} = n_T/t_h$ being the maximum uptake rate (achieved when all transporters are engaged), and $k_T = [1/(k_c t_h)]$ being equivalent to the nutrient concentration at the cell surface at which the uptake rate is half the maximum value. Although Equation 18.1.2 has the convenient Michaelis-Menten form, the substrate concentration is inconveniently that at the cell surface.

The next step is to determine the expected nutrient concentration at the cell surface, S_0, conditional on the measurable concentration in the bulk medium, S_∞. Pasciak and Gavis (1974) noted that at steady state, the transport-limited flux rate into the cell (noted above) must be equivalent to the delivery rate of the nutrient to the cell surface. The latter can be obtained by use of Fick's law (Foundations 7.2),

which states that the flux rate of a diffusing substrate across a point is equal to the product of the concentration gradient at that point and the diffusion coefficient,

$$F = -D \cdot (\partial S/\partial d)|_{d=r_e}, \tag{18.1.3a}$$

where D is the diffusion constant for the substrate, r_e is the effective radius of the cell (which can be obtained from the cell volume, assuming a sphere), and d is the distance from the center of the cell. To obtain the concentration gradient, we assume an asymptotic approach to the bulk fluid concentration, S_∞, with distance d, starting with the concentration at the cell surface, S_0,

$$S_d = S_0 + (S_\infty - S_0)\left(1 - \frac{r_e}{d}\right), \tag{18.1.3b}$$

giving

$$\frac{\partial S_d}{\partial d} = \frac{r_e(S_\infty - S_0)}{d^2}. \tag{18.1.3c}$$

After substitution into Equation 18.1.3a, with $d = r_e$, the flux per unit surface area of the sphere is found to be

$$F = D(S_\infty - S_0)/r_e, \tag{18.1.3d}$$

and multiplication by the cell surface area $4\pi r_e^2$ yields

$$V = (4\pi r_e)D(S_\infty - S_0). \tag{18.1.3e}$$

This shows that the total flux rate to the cell is proportional to r_e, rather than the surface area of the cell, because of the inverse relationship between the concentration gradient and r_e.

Often Equation 18.1.3e is multiplied by a dimensionless Sherwood number (Sh), which accounts for effects on the diffusion rate resulting from the deviation of the actual cell shape from a sphere and on other active processes that magnify the movement of substrate molecules relative to the case of pure diffusion, including swimming. In other words, Sh is defined as the ratio of the realized rate of uptake to the expectation under diffusion alone. Letting the Péclet number, $Pe = 2r_e v/D$, where $2r_e$ is the length of the cell, v the velocity, and D the diffusion coefficient, $Sh \simeq [1 + (1 + 2Pe)^{1/3}]/2$ (Guasto et al. 2012). Equation 18.1.3e assumes $Sh = 1$, and for the remaining formulae, we will suppress the use of Sh, noting that where desired it can simply be a prefactor for D.

Finally, rearranging Equation 18.1.3e to solve for S_0 and substituting the latter into Equation 18.1.2 yields the expected uptake rate

$$V = \frac{V_{\max}(V - D'S_\infty)}{V + (k_T - S_\infty)D'}, \tag{18.1.4a}$$

where $D' = D(4\pi r_e)$. Although Equation 18.1.4a is a quadratic equation whose full solution for V is somewhat complicated, Armstrong (2008) found that a close approximation is provided by

$$V \simeq \frac{V_{\max}S_\infty}{k_T + [V_{\max}/(4\pi D)] + S_\infty}. \tag{18.1.4b}$$

Note that this expression has the same form as Equation 18.1.2, with the relevant nutrient concentration now being that in the bulk medium S_∞, and the half-saturation constant being equal to $k_T + [V_{\max}/(4\pi D)]$.

The overall utility of this approach is that it provides a mechanistic understanding of uptake kinetics in terms of both the cellular features, i.e., number, affinity, and handling time of transporters (n_T, k_c, and t_h), and the additional factors influencing

the magnitude of the diffusive boundary around the cell (embodied in the parameter D). Summarizing from above

$$V_{\max} = \frac{n_T}{t_h}, \tag{18.1.5a}$$

$$k_S = \frac{1}{t_h}\left(\frac{1}{k_c} + \frac{n_T}{4\pi D}\right), \tag{18.1.5b}$$

which further implies an uptake affinity described by

$$\frac{V_{\max}}{k_S} = \frac{(4\pi D)n_T}{(4\pi D/k_c) + n_T}. \tag{18.1.5c}$$

To gain some appreciation for the degree to which swimming can enhance nutrient uptake, recall from Figure 7.8 that $D \sim 10^3 \mu\text{m}^2/\text{sec}$ for small ions. From Figure 16.4 a typical swimming speed for a bacterial cell with volume 1 μm^3 (which implies $2r_e \simeq 1.2$ μm) is $v = 50\,\mu\text{m/sec}$. This implies a Péclet number of 0.06, and a Sherwood number equal to 1.02, i.e., a 2% increase in the rate of nutrient uptake. For a eukaryotic cell of volume 10^4 μm^3 ($2r_e \simeq 120$ μm) and velocity $300\,\mu\text{m/sec}$, the Péclet number becomes 36, yielding a Sherwood number of 2.6. Thus, by breaking down the diffusion barrier by swimming, large (phytoplankton-sized) cells are capable of a substantial increase in the rate of nutrient uptake. This, of course, needs to be tempered by the increased cost of swimming.

Foundations 18.2. Encounter and capture rates. Ingestion rates are functions of both the rates at which cells physically encounter molecules (or larger prey items) and the subsequent efficiency of particle capture. The preceding theory simply treated the capture rate (per unit substrate concentration) as a fixed constant, but here we go further in mechanistic terms by considering the roles played by the rate of movement of the consumer and its substrate, the size of the cell, and the number of receptors on the surface (transporters) used in capturing the substrate. First, we consider the encounter rate, and then the efficiency of capture, the product of which can be viewed as the capture rate k_c.

In Foundations 7.2, it was shown that the rate of encounter between two passively diffusing particles is of the form

$$k_e = 4\pi RD, \tag{18.2.1a}$$

where R is the sum of the radii of the two particles, and D is the sum of their diffusion coefficients. After defining the diffusion coefficients in terms of particle radii, and assuming one particle (in this case, the consumer) is much larger than the other, this leads to

$$k_e \simeq \left(\frac{2k_BT}{3\eta}\right)\left(\frac{r_c}{r_n}\right), \tag{18.2.1b}$$

where k_B is the Boltzmann constant, T the temperature, η the viscosity of the medium, and r_c and r_n are the radii of the consumer cell and the nutrient particle. In this case of passive diffusion, the encounter rate is directly proportional to the width of the consumer cell (here assumed to be a sphere).

Suppose now that the consumer and its prey are capable of swimming at rates well beyond the diffusion rates. Then, each particle can be viewed as sweeping through a cylinder at a rate proportional to the square of the radius of the particle and the

respective swimming velocity (v_c and v_n). Under the assumption of random swimming patterns,

$$k_e = \frac{\pi R^2[(v_c + v_n)^3 - (v_c - v_n)^3]}{6 v_c v_n}, \tag{18.2.2a}$$

where R is now taken to be the encounter radius of consumer and substrate, which with a sensory system in the former might exceed the sum $(r_c + r_n)$ (Gerritsen and Strickler 1977). Assuming the prey is a passive nutrient molecule, such that $v_c \gg v_n$, this expression reduces to

$$k_e = \pi R^2 v_c, \tag{18.2.2b}$$

the area of a circle of radius R times the speed of the consumer. Thus, active swimming greatly increases the encounter rate, as this is now proportional to the square of the radius of the consumer. If turbulence contributes to movement of the consumer and/or substrate, this can be accommodated by addition of an appropriate constant to v_c (Rothschild and Osborn 1988; Evans 1989).

One limitation of these expressions is the assumption of no back-tracking on the part of the consumer, such that the same nutrient concentration is always being encountered, as might be the case if the consumer never changed direction. If, on the other hand, the direction of movement changes stochastically, the consumer will occasionally encounter an already explored patch. In this case, Equation 18.2.1a again applies, but with D redefined to be an effective diffusion coefficient. For example, in the case of run-and-tumble motion (Foundations 16.2), $D = v_c^2 \overline{\tau}/(3(1 - \overline{c})$, where $\overline{\tau}$ is the mean time between switching directions, and $\overline{c}$ is the average cosine of the angular change in direction, Equation 18.2.1a expands to

$$k_e = \frac{4\pi R v_c^2 \overline{\tau}}{3(1 - \overline{c})}, \tag{18.2.2c}$$

with the encounter rate again being linear in R (Visser and Kiørboe 2006).

If the consumer cell were 100% efficient at capturing particles upon encounter, the consumption rate would simply be proportional to the encounter rate and the substrate concentration (assuming nonsaturating conditions). However, nutrient uptake generally can only be accomplished when substrate molecules encounter particular receptors on the cell surface. Thus, we must further consider the capture efficiency, an issue first tackled in the pioneering work of Berg and Purcell (1977).

The central idea is that conditional upon an encounter, if a particle is not captured by a receptor, it will still diffuse around in the vicinity of the cell for quite some time, providing additional opportunities for proper engagement. Letting s be the radius of a receptor, with N of these distributed over the surface of the cell, the total area of receptors is $\pi N s^2$, and the probability that a random encounter does not hit a receptor is one minus the fraction of cell surface occupied by repeats,

$$P_0 = 1 - \frac{N s^2}{4 r_c^2}. \tag{18.2.3}$$

Assuming each fresh (independent) encounter of the cell starts at approximate distance s from the cell surface, the probability that the particle will be captured anew and not lost forever is

$$P_s = \frac{r_c}{r_c + s}. \tag{18.2.4}$$

The probability that the particle eventually escapes after a series of encounters is then

$$P_{\text{esc}} = \sum_{i=0}^{\infty} P_0^i P_s^i (1 - P_s) = \frac{1 - P_s}{1 - P_0 P_s}, \tag{18.2.5}$$

which leads to the probability of capture

$$P_{\rm cap} = 1 - P_{\rm esc} = \frac{Ns}{4r_c + Ns}. \tag{18.2.6}$$

The rate of successful encounters (the capture rate) is then the product $k_e P_{\rm cap}$.

This result provides insight into the degree to which a cell membrane needs to be populated by receptors to maintain a high probability of capture of encountered particles. Equation 18.2.6 shows that the probability of capture reaches 50% when the number of receptors per cell is $N = 4r_c/s$, which would occupy $(\pi s^2)(4r_c/s)$ of the total cell surface area $(4\pi r_c^2)$, implying a fractional coverage of s/r_c. Thus, as receptor diameters are $\ll r_c$, only a small fraction of the cell surface needs to be occupied by receptors to ensure a high capture efficiency.

As channels are the sites of nutrient uptake, but require nutrients for their own production, a key remaining problem is to determine the break-point beyond which the cost of channel production offsets the benefits of nutrient uptake.

Foundations 18.3. The cost of osmoregulation. The cytoplasm of cells is almost always hyperosmotic with respect to the surrounding fluid, causing a tendency for water molecules to flow through the partially permeable cell membrane. Here, we wish to calculate the energy required to maintain the hyperosmotic state of cells. The pressure difference across a membrane can be computed with the van't Hoff equation,

$$\Delta P = \Delta C \cdot k_B T, \tag{18.3.1}$$

where ΔC is the difference in the concentration of solute molecules across the membrane, k_B is the Boltzmann constant, and T is the temperature (in Kelvins). For most biological temperatures $k_B T \simeq 4.1 \times 10^{-21}$ Joules (1 Joule = 1 kg $\cdot$ M^2 $\cdot$ sec^{-2} = 0.00024 kcal). As an example, an approximate osmolarity of freshwater (summed over all solutes) is 2 mM/liter, or equivalently 2 osmol/M^3. Considering a typical cell with a cytoplasmic osmolarity of 100 osmol/M^3, and multiplying by Avogadro's number of molecules/mol, $\Delta C = 590 \times 10^{23}$ molecules/M^3, and multiplying by $k_B T$ yields $\Delta P = 242,000$ Joules/M^3.

The flow rate across a membrane is equal to the product of the pressure difference, the hydraulic conductivity (L_p), and the membrane surface area (A),

$$\Delta F = \Delta P \cdot L_p \cdot A, \tag{18.3.2}$$

where L_p has units of M^4 $\cdot$ sec^{-1} $\cdot$ Joules^{-1} when ΔP is in units of Joules/M^3, yielding ΔF in units of M^3/sec.

To understand the challenge that osmotic pressure imposes upon cells, consider that an average freshwater eukaryote has a cell-membrane conductivity $L_p \simeq 7 \times 10^{-15}$ M^4 $\cdot$ sec^{-1} $\cdot$ Joules^{-1} (Raven 1982; Hellebust et al. 1989). Assuming a spherical cell with volume 1000 μm^3, the surface area is $A = 482$ μm^2, and substitution into Equation (18.3.2) leads to a predicted water intake of $\sim 7 \times 10^4$ μm^3/day, i.e., a daily volumetric increase equal to 70$\times$ the cell volume. To maintain cell homeostasis, this is also the amount of water that must be pumped out of the cell per day.

As the mechanism by which cells expel water is not fully understood, the energy required to maintain osmotic balance remains somewhat uncertain. However, Raven (1982) provides reasoning that suggests an energetic cost of $\sim$ 100 mol ATP hydrolyses/M^3. Using this as an approximation, the 1000 μm^3 cell just noted would

require $\sim 4 \times 10^{12}$ ATP hydrolyses/day for pumping. From Chapter 3, using the formula of Lynch and Marinov (2015), the daily total maintenance cost for a cell of this size is $\sim 4 \times 10^{12}$ ATP hydrolyses. There are a number of uncertainties in these calculations, but assuming they are roughly correct, the implication is that a substantial fraction of cellular maintenance costs in eukaryotic cells derive from the regulation of osmotic balance.

Literature Cited

Abascal, F., I. Irisarri, and R. Zardoya. 2014. Diversity and evolution of membrane intrinsic proteins. Biochim. Biophys. Acta 1840: 1468-1481.

Acquisti, C., S. Kumar, and J. J. Elser. 2009. Signatures of nitrogen limitation in the elemental composition of the proteins involved in the metabolic apparatus. Proc. Biol. Sci. 276: 2605-2610.

Alves, R., and M. A. Savageau. 2005. Evidence of selection for low cognate amino acid bias in amino acid biosynthetic enzymes. Mol. Microbiol. 56: 1017-1034.

Armstrong, R. A. 2008. Nutrient uptake rate as a function of cell size and surface transporter density: a Michaelis-like approximation to the model of Pasciak and Gavis. Deep Sea Research Part I: Oceanogr. Res. Papers 55: 1311-1317.

Ashida, H., A. Danchin, and A. Yokota. 2005. Was photosynthetic RuBisCO recruited by acquisitive evolution from RuBisCO-like proteins involved in sulfur metabolism? Res. Microbiol. 156: 611-618.

Badger, M. R., T. J. Andrews, S. M. Whitney, M. Ludwig, et al. 1998. The diversity and coevolution of Rubisco, plastids, pyrenoids, and chloroplast-based CO_2-concentrating mechanisms in algae. Can. J. Botany 76: 1052-1071.

Bar-On, Y. M., and R. Milo. 2019. The global mass and average rate of rubisco. Proc. Natl. Acad. Sci. USA 116: 4738-4743.

Baudouin-Cornu, P., Y. Surdin-Kerjan, P. Marlière, and D. Thomas. 2001. Molecular evolution of protein atomic composition. Science 293: 297-300.

Beardall, J., and M. Giordano. 2002. Ecological implications of microalgal and cyanobacterial CO_2 concentrating mechanisms, and their regulation. Func. Plant Biol. 29: 335-347.

Berg, H. C., and E. M. Purcell. 1977. Physics of chemoreception. Biophys. J. 20: 193-219.

Berg, I. A., D. Kockelkorn, W. H. Ramos-Vera, R. F. Say, J. Zarzycki, M. Hügler, B. E. Alber, and G. Fuchs. 2010. Autotrophic carbon fixation in archaea. Nat. Rev. Microbiol. 8: 447-460.

Blount, Z. D., J. E. Barrick, C. J. Davidson, and R. E. Lenski. 2012. Genomic analysis of a key innovation in an experimental *Escherichia coli* population. Nature 489: 513-518.

Bosdriesz, E., M. T. Wortel, J. R. Haanstra, M. J. Wagner, P. de la Torre Cortés, and B. Teusink. 2018. Low affinity uniporter carrier proteins can increase net substrate uptake rate by reducing efflux. Sci. Rep. 8: 5576.

Bouget, F. Y., M. Lefranc, Q. Thommen, B. Pfeuty, J. C. Lozano, P. Schattab, H. Botebo, and V. Vergé. 2014. Transcriptional versus non-transcriptional clocks: a case study in *Ostreococcus*. Mar. Genomics 14: 17-22.

Bremer, E., and R. Krämer. 2019. Responses of microorganisms to osmotic stress. Annu. Rev. Microbiol. 73: 313-334.

Brown, N. J., C. A. Newell, S. Stanley, J. E. Chen, A. J. Perrin, K. Kajala, and J. M. Hibberd. 2011. Independent and parallel recruitment of preexisting mechanisms underlying C_4 photosynthesis. Science 331: 1436-1439.

Brunner, M., and M. Merrow. 2008. The green yeast uses its plant-like clock to regulate its

animal-like tail. Genes Dev. 22: 825-831.

Buchmann, K., and B. Becker. 2009. The system of contractile vacuoles in the green alga *Mesostigma viride* (Streptophyta). Protist 160: 427-443.

Cardona, T. 2015. A fresh look at the evolution and diversification of photochemical reaction centers. Photosynth. Res. 126: 111-134.

Cardona, T., J. W. Murray, and A. W. Rutherford. 2015. Origin and evolution of water oxidation before the last common ancestor of the cyanobacteria. Mol. Biol. Evol. 32: 1310-1328.

Chakraborty, S., L. T. Nielsen, and K. H. Andersen. 2017. Trophic strategies of unicellular plankton. Am. Nat. 189: E77-E90.

Chen, M., and R. E. Blankenship. 2011. Expanding the solar spectrum used by photosynthesis. Trends Plant Sci. 16: 427-431.

Chew, J., E. Leypunskiy, J. Lin, A. Murugan, and M. J. Rust. 2018. High protein copy number is required to suppress stochasticity in the cyanobacterial circadian clock. Nat. Commun. 9: 3004.

Claessen, D., and J. Errington. 2019. Cell wall deficiency as a coping strategy for stress. Trends Microbiol. 27: 1025-1033.

Collos, Y., A. Vaquer, and P. Souchou. 2005. Acclimation of nitrate uptake by phytoplankton to high substrate levels. J. Phycol. 41: 466-478.

Delwiche, C. F., and J. D. Palmer. 1996. Rampant horizontal transfer and duplication of rubisco genes in eubacteria and plastids. Mol. Biol. Evol. 13: 873-882.

de Queiroz, J. H., J.-L. Uribelarrea, and A. Pareilleux. 1993. Estimation of the energetic biomass yield and efficiency of oxidative phosphorylation in cell-recycle cultures of *Schizosaccharomyces pombe.* Applied Microbiol. Biotech. 39: 609-614.

Driessen, A. J., B. P. Rosen, and W. N. Konings. 2000. Diversity of transport mechanisms: common structural principles. Trends Biochem. Sci. 25: 397-401.

Edwards, K. F., M. K. Thomas, C. A. Klausmeier, and E. Litchman. 2012. Allometric scaling and taxonomic variation in nutrient utilization traits and maximum growth rate of phytoplankton. Limnol. Oceanogr. 57: 554-566.

Eelderink-Chen, Z., G. Mazzotta, M. Sturre, J. Bosman, T. Roenneberg, and M. Merrow. 2010. A circadian clock in *Saccharomyces cerevisiae.* Proc. Natl. Acad. Sci. USA 107: 2043-2047.

Eide, D. J. 2012. An "inordinate fondness for transporters" explained? Science Signaling 5: 5.

Erb, T. J., and J. Zarzycki. 2018. A short history of RubisCO: the rise and fall (?) of nature's predominant CO(2) fixing enzyme. Curr. Opin. Biotechnol. 49: 100-107.

Errington, J. 2017. Cell wall-deficient, L-form bacteria in the 21st century: a personal perspective. Biochem. Soc. Trans. 45: 287-295.

Errington, J., K. Mickiewicz, Y. Kawai, and L. J. Wu. 2016. L-form bacteria, chronic diseases and the origins of life. Philos. Trans. R. Soc. Lond. B Biol. Sci. 371: 20150494.

Evans, G. T. 1989. The encounter speed of moving predator and prey. J. Plank. Res. 11: 415-417.

Fagerbakke, K. M., M. Heldal, and S. Norland. 1996. Content of carbon, nitrogen, oxygen, sulfur and phosphorus in native aquatic and cultured bacteria. Aquatic Microb. Ecol. 10: 15-27.

Fagerbakke, K. M., S. Norland, and M. Heldal. 1999. The inorganic ion content of native aquatic bacteria. Can. J. Microbiology 45: 304-311.

Falkowski, P. G., and J. A. Raven. 2007. Aquatic Photosynthesis. 2nd Ed. Princeton Univ. Press, Princeton, NJ.

Feeney, K. A., L. L. Hansen, M. Putker, C. Olivares-Yañez, J. Day, L. J. Eades, L. F. Larrondo, N. P. Hoyle, J. S. O'Neill, and G. van Ooijen. 2016. Daily magnesium fluxes regulate cellular timekeeping and energy balance. Nature 532: 375-379.

Finlay, B. J., and G. Uhlig. 1981. Calorific and carbon values of marine and freshwater Protozoa. Helgoländer Meeresuntersuchungen 34: 401-412.

Fischer, W. W., J. Hemp, and J. E. Johnson. 2016. Evolution of oxygenic photosynthesis. Annu. Rev. Earth Planetary Sci. 44: 647-683.

Flamholz, A. I., N. Prywes, U. Moran, D. Davidi, Y. M. Bar-On, L. M. Oltrogge, R. Alves, D. Savage, and R. Milo. 2019. Revisiting trade-offs between Rubisco kinetic parameters. Biochemistry 58: 3365-3376.

Folsom, J. P., and R. P. Carlson. 2015. Physiological, biomass elemental composition and proteomic analyses of *Escherichia coli* ammonium-limited chemostat growth, and comparison with iron- and glucose-limited chemostat growth. Microbiology 161: 1659-1670.

Fuchs, G. 2011. Alternative pathways of carbon dioxide fixation: insights into the early evolution of life? Annu. Rev. Microbiol. 65: 631-658.

Gerritsen, J., and J. R. Strickler 1977. Encounter probabilities and community structure in zooplankton: a mathematical model. J. Fish. Res. Bd. Canada 34: 73-82.

Gomez-Fernandez, B. J., E. Garcia-Ruiz, J. Martin-Diaz, P. Gomez de Santos, P. Santos-Moriano, F. J. Plou, A. Ballesteros, M. Garcia, M. Rodriguez, V. A. Risso, et al. 2018. Directed *in vitro* evolution of Precambrian and extant Rubiscos. Sci. Rep. 8: 5532.

Greganova, E., M. Steinmann, P. Mäser, and N. Fankhauser. 2013. *In silico* ionomics segregates parasitic from free-living eukaryotes. Genome Biol. Evol. 5: 1902-1909.

Guasto, J. S., R. Rusconi, and R. Stocker. 2012. Fluid mechanics of planktonic microorganisms. Ann. Rev. Fluid Mechanics 44: 373-400.

Gudelj, I., R. E. Beardmore, S. S. Arkin, and R. C. MacLean. 2007. Constraints on microbial metabolism drive evolutionary diversification in homogeneous environments. J. Evol. Biol. 20: 1882-1889.

Heldal, M., D. J. Scanlan, S. Norland, F. Thingstad, and N. H. Mann. 2003. Elemental composition of single cells of various strains of marine *Prochlorococcus* and *Synechococcus* using Xray microanalysis. Limnol. Oceanogr. 48: 1732-1743.

Hellebust, J. A., T. Mérida, and I. Ahmad. 1989. Operation of contractile vacuoles in the euryhaline green flagellate *Chlamydomonas pulsatilla* (Chlorophyceae) as a function of salinity. Mar. Biol. 100: 373-379.

Helling, R. B., C. N. Vargas, and J. Adams. 1987. Evolution of *Escherichia coli* during growth in a constant environment. Genetics 116: 349-358.

Hennaut, C., F. Hilger, and M. Grenson. 1970. Space limitation for permease insertion in the cytoplasmic membrane of *Saccharomyces cerevisiae*. Biochem. Biophys. Res. Commun. 39:

666-671.

Heyduk, K., J. J. Moreno-Villena, I. S. Gilman, P. A. Christin, and E. J. Edwards. 2019. The genetics of convergent evolution: insights from plant photosynthesis. Nat. Rev. Genet. 20: 485-493.

Higgins, C. F. 1992. ABC transporters: from microorganisms to man. Annu. Rev. Cell Biol. 8: 67-113.

Hill, J. F., and Govindjee. 2014. The controversy over the minimum quantum requirement for oxygen evolution. Photosynth. Res. 122: 97-112.

Ho, K. P., and W. J. Payne. 1979. Assimilation efficiency and energy contents of prototrophic bacteria. Bioctech. Bioeng. 21: 787-802.

Ho, T.Y., A. Quigg, Z. V. Finkel, A. J. Milligan, K. Wyman, P. G. Falkowski, and F. M. M. Morel. 2003. The elemental composition of some marine phytoplankton. J. Phycol. 39: 1145-1159.

Hobson, L.A., and K. P. Guest. 1983. Values of net compensation irradiation and their dependence on photosynthetic efficiency and respiration in marine unicellular algae. Mar. Biol. 74: 1-7.

Holtzendorff, J., F. Partensky, D. Mella, J. F. Lennon, W. R. Hess, and L. Garczarek. 2008. Genome streamlining results in loss of robustness of the circadian clock in the marine cyanobacterium *Prochlorococcus marinus* PCC 9511. J. Biol. Rhythms 23: 187-199.

Hong, C. I., J. Zámborszky, M. Baek, L. Labiscsak, K. Ju, et al. 2014. Circadian rhythms synchronize mitosis in *Neurospora crassa*. Proc. Natl. Acad. Sci. USA 111: 1397-1402.

Kageyama, H., T. Nishiwaki, M. Nakajima, H. Iwasaki, T. Oyama, and T. Kondo. 2006. Cyanobacterial circadian pacemaker: Kai protein complex dynamics in the KaiC phosphorylation cycle *in vitro*. Mol. Cell. 23: 161-171.

Kapralov, M. V., and D. A. Filatov. 2007. Widespread positive selection in the photosynthetic Rubisco enzyme. BMC Evol. Biol. 7: 73.

Kruckeberg, A. L., L. Ye, J. A. Berden, and K. van Dam. 1999. Functional expression, quantification and cellular localization of the Hxt2 hexose transporter of *Saccharomyces cerevisiae* tagged with the green fluorescent protein. Biochem. J. 339: 299-307.

Lambert, G., J. Chew, and M. J. Rust. 2016. Costs of clock-environment misalignment in individual cyanobacterial cells. Biophys. J. 111: 883-891.

Lange, H. C., and J. J. Heijnen. 2001. Statistical reconciliation of the elemental and molecular biomass composition of *Saccharomyces cerevisiae*. Biotechnol. Bioeng. 75: 334-344.

Lear, J. D., Z. R. Wasserman, and W. F. DeGrado. 1988. Synthetic amphiphilic peptide models for protein ion channels. Science 240: 1177-1181.

Levy, S., M. Kafri, M. Carmi, and N. Barkai. 2011. The competitive advantage of a dual-transporter system. Science 334: 1408-1412.

Leypunskiy, E., J. Lin, H. Yoo, U. Lee, A. R. Dinner, and M. J. Rust. 2017. The cyanobacterial circadian clock follows midday *in vivo* and *in vitro*. Elife 6: e23539.

Litchman, E., C. A. Klausmeier, O. M. Schofield, and P. G. Falkowski. 2007. The role of functional traits and tradeoffs in structuring phytoplankton communities: scaling from cellular to ecosystem level. Ecol. Letters 10: 1170-1181.

Lomas, M. W., J. A. Bonachela, S. A. Levin, and A. C. Martiny. 2014. Impact of ocean phytoplankton diversity on phosphate uptake. Proc. Natl. Acad. Sci. USA 111: 17540-17545.

Loukin, S. H., M. M. Kuo, X. L. Zhou, W. J. Haynes, C. Kung, and Y. Saimi. 2005. Microbial K+ channels. J. Gen. Physiol. 125: 521-527.

Lycklama A Nijeholt, J. A., R. Vietrov, G. K. Schuurman-Wolters, and B. Poolman. 2018. Energy coupling efficiency in the Type I ABC transporter GlnPQ. J. Mol. Biol. 430: 853-866.

Lynch, M., and G. K. Marinov. 2015. The bioenergetic costs of a gene. Proc. Natl. Acad. Sci. USA 112: 15690-15695.

Lynch, M., W.-C. Ho, and C. P. Kempes. 2020. Evolutionary scaling of maximum growth rates with the drift barrier. (Submitted to Nature Ecol. Evol.)

Lynn, D. H. 1982. Dimensionality and contractile vacuole function in ciliated protozoa. J. Exp. Zool. 223: 219-229.

Lyons, T. W., C. T. Reinhard, and N. J. Planavsky. 2014. The rise of oxygen in Earth's early ocean and atmosphere. Nature 506: 307-315.

Maharjan, R. P., S. Seeto, and T. Ferenci. 2007. Divergence and redundancy of transport and metabolic rate-yield strategies in a single *Escherichia coli* population. J. Bacteriol. 189: 2350-2358.

Marañón, E. 2015. Cell size as a key determinant of phytoplankton metabolism and community structure. Ann. Rev. Mar. Sci. 7: 241-264.

Mazel, D., and P. Marlière. 1989. Adaptive eradication of methionine and cysteine from cyanobacterial light-harvesting proteins. Nature 341: 245-248.

Melis, A. 2009. Solar energy conversion efficiencies in photosynthesis: minimizing the chlorophyll antennae to maximize efficiency. Plant Science 177: 272-280.

Menden-Deuer, S., and E. J. Lessard. 2000. Carbon to volume relationships for dinoflagellates, diatoms, and other protist plankton. Limnol. Oceanogr. 45: 569-579.

Morse, D., P. Salois, P. Markovic, and J. W. Hastings. 1995. A nuclear-encoded form II RuBisCO in dinoflagellates. Science 268: 1622-1624.

Mulkidjanian, A. Y., M. Y. Galperin, and E. V. Koonin. 2009. Co-evolution of primordial membranes and membrane proteins. Trends Biochem. Sci. 34: 206-215.

Naftalin, R. J., N. Green, and P. Cunningham. 2007. Lactose permease H+-lactose symporter: mechanical switch or Brownian ratchet? Biophys. J. 92: 3474-3491.

Nakajima, M., K. Imai, H. Ito, T. Nishiwaki, Y. Murayama, H. Iwasaki, T. Oyama, and T. Kondo. 2005. Reconstitution of circadian oscillation of cyanobacterial KaiC phosphorylation *in vitro*. Science 308: 414-415.

Noordally, Z. B., and A. J. Millar. 2015. Clocks in algae. Biochemistry 54: 171-183.

Nozaki, Y. 1997. A fresh look at element distribution in the North Pacific. EOS 78: 221-223.

O'Neill, J. S., G. van Ooijen, L. E. Dixon, C. Troein, F. Corellou, F. Y. Bouget, A. B. Reddy, and A. J. Millar. 2011. Circadian rhythms persist without transcription in a eukaryote. Nature 469: 554-558.

Oren, A. 1999. Bioenergetic aspects of halophilism. Microbiol. Mol. Biol. Rev. 63: 334-348.

Partch, C. L., C. B. Green, and J. S. Takahashi. 2014. Molecular architecture of the mammalian circadian clock. Trends Cell Biol. 24: 90-99.

Pasciak, W. J., and J. Gavis. 1974. Transport limitation of nutrient uptake in phytoplankton. Limnol. Oceanogr. 19: 881-888.

Pattanayak, G. K., G. Lambert, K. Bernat, and M. J. Rust. 2015. Controlling the cyanobacterial clock by synthetically rewiring metabolism. Cell Rep. 13: 2362-2367.

Patzlaff, J. S., T. van der Heide, and B. Poolman. 2003. The ATP/substrate stoichiometry of the ATP-binding cassette (ABC) transporter OpuA. J. Biol. Chem. 278: 29546-29551.

Phillips, R., and R. Milo. 2009. A feeling for the numbers in biology. Proc. Natl. Acad. Sci. USA 106: 21465-21471.

Phong, C., J. S. Markson, C. M. Wilhoite, and M. J. Rust. 2013. Robust and tunable circadian rhythms from differentially sensitive catalytic domains. Proc. Natl. Acad. Sci. USA 110: 1124-1129.

Pittayakanchit, W., Z. Lu, J. Chew, M. J. Rust, and A. Murugan. 2018. Biophysical clocks face a trade-off between internal and external noise resistance. Elife 7: e37624.

Pohorille, A., K. Schweighofer, and M. A. Wilson. 2005. The origin and early evolution of membrane channels. Astrobiology 5: 1-17.

Purcell, E. M. 1977. Life at low Reynolds number. Amer. J. Physics 45: 3.

Raven, J. A. 1982. The energetics of freshwater algae: energy requirements for biosynthesis and volume regulation. New Phytol. 92: 1-20.

Raven, J. A. 2009. Contributions of anoxygenic and oxygenic phototrophy and chemolithotrophy to carbon and oxygen fluxes in aquatic environments. Aquatic Microb. Ecol. 56: 177-192

Raven, J. A., J. Beardall, and P. Sánchez-Baracaldo. 2017. The possible evolution and future of CO_2-concentrating mechanisms. J. Exp. Bot. 68: 3701-3716.

Raven, J. A., and M. A. Doblin. 2014. Active water transport in unicellular algae: where, why, and how. J. Exp. Bot. 65: 6279-6292.

Redfield, A. C. 1934. the proportions of organic derivatives in sea water and their relation to the composition of plankton. James Johnstone Memorial Volume 176-192.

Roels, J. A. 1980. Application of macroscopic principles to microbial metabolism. Biotech. Bioeng. 22: 2457-2514.

Roenneberg, T., and M. Merrow. 2001. Circadian systems: different levels of complexity. Philos. Trans. R. Soc. Lond. B Biol. Sci. 356: 1687-1696.

Rothschild, B. J., and T. R. Osborn. 1988. Small-scale turbulence and plankton contact rates. J. Plank. Res. 10: 465-474.

Samani, P., and G. Bell. 2016. Experimental evolution of the grain of metabolic specialization in yeast. Ecol. Evol. 6: 3912-3922.

Sartor, F., Z. Eelderink-Chen, B. Aronson, J. Bosman, L. E. Hibbert, et al. 2019. Are there circadian clocks in non-photosynthetic bacteria? Biology (Basel) 8: E41.

Savir, Y., E. Noor, R. Milo, and T. Tlusty. 2010. Cross-species analysis traces adaptation of Rubisco toward optimality in a low-dimensional landscape. Proc. Natl. Acad. Sci. USA 107:

3475-3480.

Shih, P. M. 2015. Photosynthesis and early Earth. Curr. Biol. 25: R855-R859.

Shih, P. M., A. Occhialini, J. C. Cameron, P. J. Andralojc, M. A. Parry, and C. A. Kerfeld. 2016. Biochemical characterization of predicted Precambrian RuBisCO. Nat. Commun. 7: 10382.

Shih, P. M., L. M. Ward, and W. W. Fischer. 2017. Evolution of the 3-hydroxypropionate bicycle and recent transfer of anoxygenic photosynthesis into the Chloroflexi. Proc. Natl. Acad. Sci. USA 114: 10749-10754.

Spreitzer, R. J., and M. E. Salvucci. 2002. Rubisco: structure, regulatory interactions, and possibilities for a better enzyme. Annu. Rev. Plant Biol. 53: 449-475.

Stevens, T. J., and I. T. Arkin. 2000. Do more complex organisms have a greater proportion of membrane proteins in their genomes? Proteins 39: 417-420.

Tcherkez, G. G., G. D. Farquhar, and T. J. Andrews. 2006. Despite slow catalysis and confused substrate specificity, all ribulose bisphosphate carboxylases may be nearly perfectly optimized. Proc. Natl. Acad. Sci. USA 103: 7246-7251.

Terauchi, K., Y. Kitayama, T. Nishiwaki, K. Miwa, Y. Murayama, T. Oyama, and T. Kondo. 2007. ATPase activity of KaiC determines the basic timing for circadian clock of cyanobacteria. Proc. Natl. Acad. Sci. USA 104: 16377-16381.

Thauer, R. K. 2007. A fifth pathway of carbon fixation. Science 318: 1732-1733.

Tortell, P. D. 2000. Evolutionary and ecological perspectives on carbon acquisition in phytoplankton. 45: 744-750.

van Ooijen, G., L. E. Dixon, C. Troein, and A. J. Millar. 2011. Proteasome function is required for biological timing throughout the twenty-four hour cycle. Curr. Biol. 21: 869-875.

Visser, A. W., and T. Kiørboe. 2006. Plankton motility patterns and encounter rates. Oecologia 148: 538-546.

von Stockar, U., and I. W. Marison. 2005. The use of calorimetry in biotechnology bioprocesses and engineering. Adv. Biochem. Eng./Biotech. Book Series 40: 93-136.

Wallin, E., and G. von Heijne. 1998. Genome-wide analysis of integral membrane proteins from eubacterial, archaean, and eukaryotic organisms. Protein Sci. 7: 1029-1038.

Waygood, E. B., and T. Steeves. 1980. Enzyme I of the phosphoenolpyruvate: sugar phosphotransferase system of *Escherichia coli.* Purification to homogeneity and some properties. Can. J. Biochem. 58: 40-48.

Williams, K., F. Percival, J. Merino, and H. A. Mooney. 1987. Estimation of tissue construction cost from heat of combustion and organic nitrogen content. Plant Cell Environ. 10: 725-734.

Woese, C. R. 1987. Bacterial evolution. Microbiol. Rev. 51: 221-271.

Woese, C. R, B. A. Debrunner-Vossbrinck, H. Oyaizu, E. Stackebrandt, and W. Ludwig. 1985. Gram-positive bacteria: possible photosynthetic ancestry. Science 229: 762-765.

Wykoff, D. D., A. H. Rizvi, J. M. Raser, B. Margolin, and E. K. O'Shea. 2007. Positive feedback regulates switching of phosphate transporters in *S. cerevisiae.* Mol. Cell. 27: 1005-1013.

Ye, L., J. A. Berden, K. van Dam, and A. L. Kruckeberg. 2001. Expression and activity of the Hxt7 high-affinity hexose transporter of *Saccharomyces cerevisiae.* Yeast 18: 1257-1267.

Young, J. N., R. E. Rickaby, M. V. Kapralov, and D. A. Filatov. 2012. Adaptive signals in algal Rubisco reveal a history of ancient atmospheric carbon dioxide. Philos. Trans. R. Soc. Lond. B Biol. Sci. 367: 483-492.

Zehr, J. P., J. S. Weitz, and I. Joint. 2017. How microbes survive in the open ocean. Science 357: 646-647.

Figure 18.1. Left) A structural explanation for the use of dual high/low-affinity transporters for nutrient uptake. Transporters can be bidirectional, in the sense that they can bind to substrates on both sides of the membrane. Hence, when nutrient concentrations are high internally and externally, rates of influx will be nearly equal to those of efflux. However, low affinity transporters require higher concentrations to become saturated, and therefore maintain larger differences between influx and eflux rates at high nutrient concentrations. **Right)** Net influx rates for transporters with different affinities are given for three substrate concentrations (solid lines). Net influx is low when k_S is low because saturation occurs at very low substrate concentrations, as the high affinity leads to near equal levels of binding on both sides of the membrane. On the other hand, with very high k_S, there is little competitive binding, but the overall influx rate is low simply because of the low absolute affinity on the external side of the membrane. Overall rates of influx increase with nutrient concentration regardless of k_S, but the optimum k_S shifts to the right (the optimum affinity is lowered) with higher concentrations. The dashed lines show the behavior that would occur with purely Michaelis-Menten uptake dynamics – the optimal k_S is always zero. Derivations and other details can be found in Bosdriesz et al. (2018).

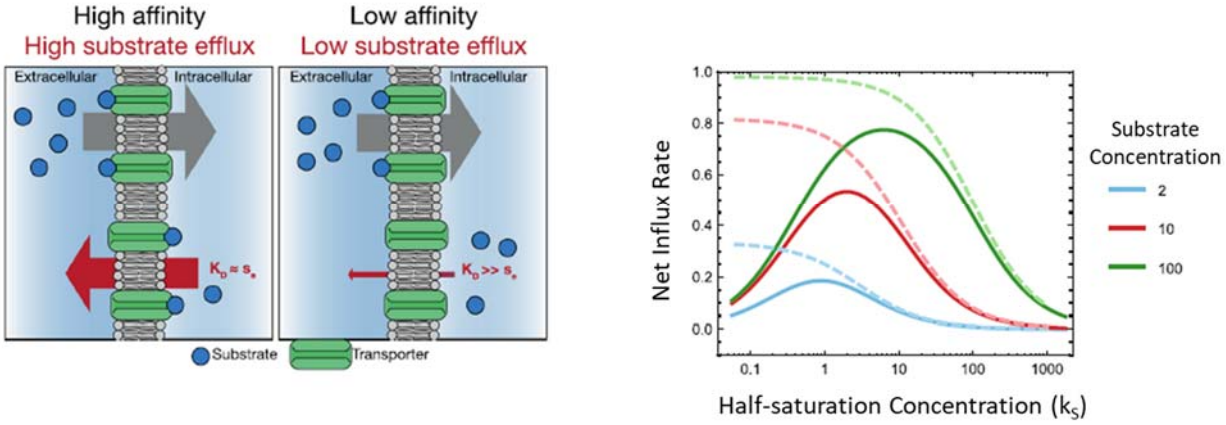

Figure 18.2. The historical record of the Earth's atmospheric CO_2 and O_2 concentrations, given as a crude idealization of patterns outlined in Shih (2015) and Raven (2017). Note that the vertical axis is on a logarithmic scale.

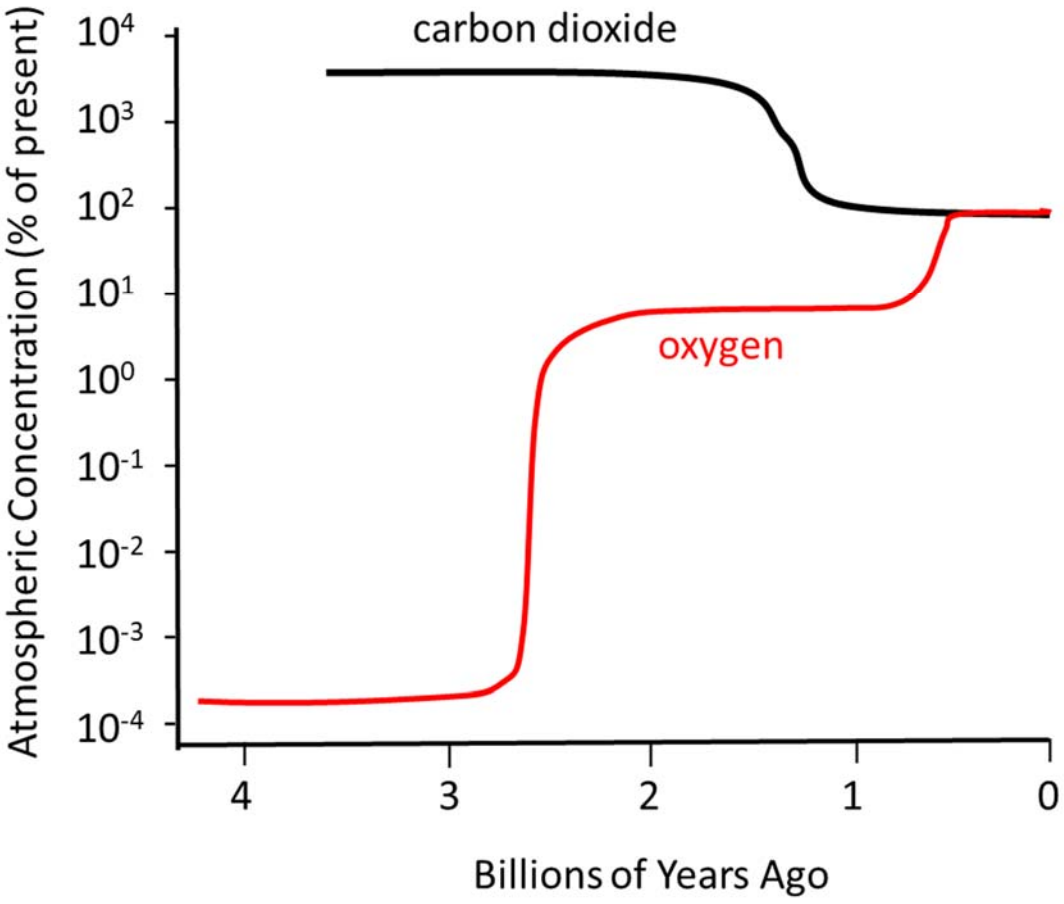

Figure 18.3. Some compatible solutes commonly deployed in osmotic regulation in prokaryotes and eukaryotes, and the biosynthetic costs per molecule (in parentheses, and in units of ATP hydrolyses). Taken from Oren (1999; his Figure 2), with the costs taken to be averages for photosynthesizers and aerobic heterotrophs.

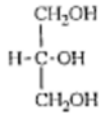

Glycerol

(27)

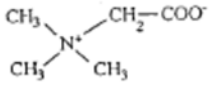

Glycine betaine

(46)

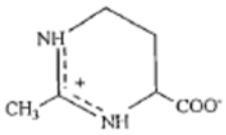

Ectoine

(46)

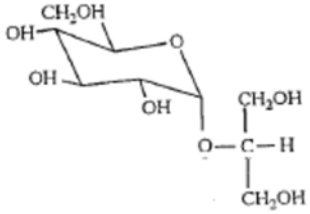

Glucosylglycerol

(76)

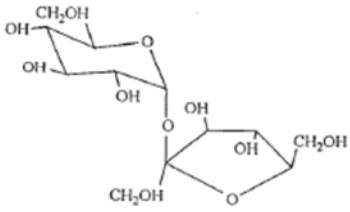

Sucrose

(95)

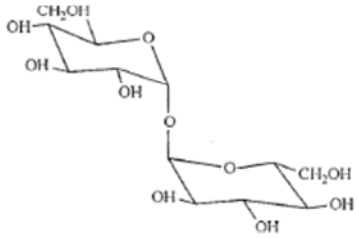

Trehalose

(95)

Figure 18.4. Left) The molecular network for the circadian clock in the cyanobacterium *Synechococcus*. Hexameric KaiC is autophosphorylated in the presence of KaiA (right), until it is joined by KaiB (left), which encourages dephosphorylation. This cyclical pattern driven by ATP results in stable oscillations. From Phong et al. (2013). **Right)** A simplified view of the vertebrate molecular clock. The heterodimeric transcription factor Clock/Bmal1 activates transcription of the Per and Cry genes, the mRNAs of which are translated in the cytoplasm. The proteins of the latter two genes then heterodimerize, return to the nucleus, and suppress their own expression. This leads to stable 24-hour cycles. From Partch et al. (2014).